

237D Fusion Technology Introduction to Solid Breeder

Jon Van Lew

March 2, 2016

Contents

1 Solid Breeder Material Technology	2
1.1 Material Requirements	3
1.1.1 Neutronics of Lithium and Lithiated Ceramics	4
1.1.2 Thermochemical Properties	5
1.1.3 Tritium Release and Recovery	7
1.1.4 Physical & Thermophysical Properties	12
1.1.5 Compatibility	13
1.1.6 Radiation Effects	13
1.1.7 Fabrication	16
1.2 Neutron Multiplication in Solid Breeders	16
2 Introduction to Solid Breeder Analysis	19
2.1 Solid Breeder Thermal Management and Imposed Temperature Window	20
2.2 Purge Gas and Coolant Flow	21
2.2.1 Purge Gas	22
2.2.2 Coolant	23
2.3 Phenomenological Properties of Packed Beds	24
2.3.1 Empirical Models for Heat Transfer Packed Beds	24
2.3.2 Experimental Measurements of Lithium Ceramics	26
2.3.3 Thermo-mechanical Interactions	29
2.3.4 Post-irradiation Experiments	31
2.4 Continuum Modeling of Packed Beds	32
2.5 Discrete Modeling of Packed Beds	33
2.5.1 Particle Dynamics	33
2.5.2 Granular Heat Transfer in DEM	36
2.5.3 DEM Example Analysis	37
2.6 Closing Remarks	42

Chapter 1

Solid Breeder Material Technology

Aside from liquid lithiums (covered in separate lectures in this course), solid lithium materials are potential candidates for tritium generation in fusion power plants. Many different potential solid materials have been studied in the past; including inter-metallic compounds (*e.g.* Li_7Pb_2), lithium oxide (Li_2O), and ternary oxides (*e.g.* Li_4SiO_4 , Li_2TiO_3 , LiAlO_2 , Li_2ZrO_3 , *etc.*). Solid breeder materials offer a number of potential safety advantages including relatively low tritium mobility and low stored chemical energy.

Over the years, the fusion community has come to recognize that lithium-based oxides (including ceramic oxides) are best candidate tritium-breeding materials for fusion reactor blankets. This conclusion is based on oxides having many desirable characteristics, such as:

- high Li density
- high melting temperature
- good tritium release (sufficiently high T release rates, low solubility, and open porosity for purging T)
- good thermophysical and thermomechanical characteristics
- ability to withstand the rigors of long-term irradiation at high temperature and under large temperature gradients
- desirable neutronics and irradiation characteristics (no bad transmutation nuclides)

- chemical stability & compatibility with structural material at operating temperatures (in particular thermal stability and chemical inertness are attractive from a safety point of view)

Calculations of other candidate materials indicate that inter-metallic compounds have unacceptable operating temperatures (exceedingly narrow temperature windows) and are unattractive for in-situ tritium recovery. In addition, the compounds of Li_7Pb_2 and $\text{Li}_{62}\text{Pb}_{38}$ were shown to vigorously react with water and do not offer significant safety advantages compared to liquid breeders. And a major emphasis of blanket/breeder design is placed on safety and environmental acceptability, with primary goals of low tritium inventory in the blanket and minimal long-lived activation products. Therefore in these notes we will not discuss the inter-metallic compounds and focus instead only on candidate materials of lithium ceramics. If you wish to read more on inter-metallics, begin with Clemmer [11] and Abdou *et al.* [3]

Finally, I've attempted to provide as succinct an introduction as possible to ceramic breeder material development and modeling without overly-sacrificing detail. In spite of my efforts, there are some topics which are not justly covered in these short chapters. As such, the references listed in the bibliography at the end of these notes can be considered a must-read list for serious newcomers to the solid breeder world.

1.1 Material Requirements

In the time since the solid breeder concept was introduced, a rich experimental database has begun to develop for a number of candidate ceramic materials. For each candidate breeder, a number of performance criteria were established in design studies in the late 1970s and early 1980s. The outcome of the studies can be summarized in the following list:

1. Neutronics
2. Thermochemical Properties
3. Tritium Release
4. Physical/Thermo-physical Properties
5. Compatibility
6. Radiation Effects
7. Fabrication

The necessity of each requirement will be discussed in brief, followed by a discussion of the analysis involved with evaluating materials for that requirement.

1.1.1 Neutronics of Lithium and Lithiated Ceramics

Neutronics requirements of candidate solid materials can be thought of as simply not getting in the way of the lithium reaction with neutrons. An important measure for lithium oxides is the lithium density in the compound. In general, lithium ceramics will almost all require neutron multiplying material to supplement the fusion neutrons for the sake of tritium breeding ratio.

To review: natural lithium occurs with the isotopic abundances of 92.58% for ^7Li and 7.42% for ^6Li . At low neutron energies, the major tritium and heat producing neutron reaction in lithium ceramics is associated with the ^6Li isotope:



The cross-section for this reaction is given in Figure 1.1. ^6Li has a very high neutron capture cross-section (3,000 barns) for thermal neutrons $E \approx 10^{-1}$ to 10^{-2} eV. Yet, at high neutron energies (14 MeV), such as those found near the first wall of a fusion reactor, the neutron cross section of ^6Li drops to less than 0.1 barn, effectively precluding the ^6Li reaction with virgin fusion neutrons. In reality, the high energy neutrons are slowed from collisions with the structural material in the first wall and blanket. Consequently, ^6Li reaction rates near the first wall are highly dependent on the ability of first walls and blankets to moderate neutron energies.

Neutron multipliers such as lead and beryllium not only moderate 14 MeV neutrons, yielding a softer neutron spectrum for increased ^6Li reactions, but also generate additional neutrons from $(n,2n)$ reactions. Neutron multiplication materials will be discussed again shortly.

^7Li interactions with neutrons, being endothermic, possesses a threshold energy below which it will not react with neutrons. It does, however, have a small but significant cross-section (around 1 barn) for neutrons with energies greater than 5 MeV. The ^7Li reaction is:



where the reaction releases a lower energy neutron which is immediately available for capture by ^6Li atoms. Due to ^7Li ability to act as neutron multiplier, Li_2O , with a high lithium atom density, is potentially capable of attaining adequate tritium breeding ratios without an external neutron multiplication material. Several atomic densities of lithium for select candidate materials are given in Figure 1.2. Aside from Li_2O , all ternary oxides require neutron multiplication due to low lithium density.

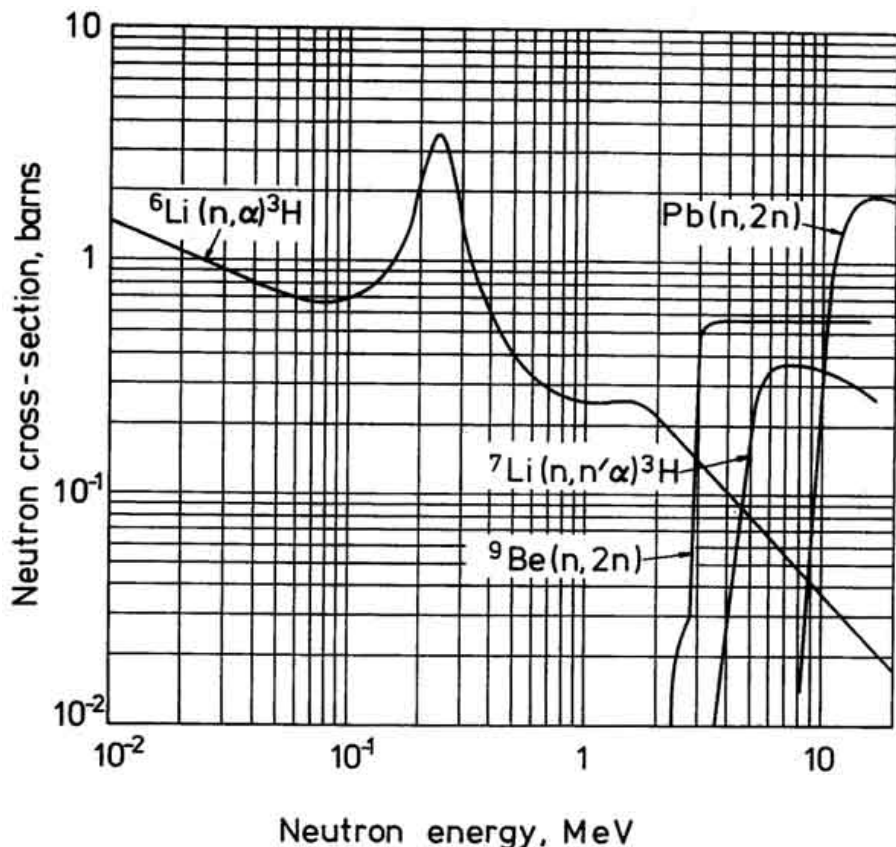
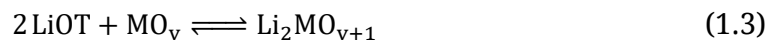


Figure 1.1: Cross-sections of various blanket materials. Note the threshold for the ^7Li and neutron multiplying reactions.

1.1.2 Thermochemical Properties

Vapor pressure, phase equilibria, thermal stability, and thermodynamics are several of the thermochemical properties important to the study of ceramic breeder materials.

A major concern of candidate materials is the solubility of tritium in the material; too high solubility will lead to unacceptable levels of tritium inventory. A simplified calculation can be performed on the lithium oxides to predict the function of T_2O partial pressure in gas phase. Assuming: 1) thermochemical data of hydrogen applies to tritium; 2) isotope effects are not considered; 3) tritium exists in the form of LiOT in solid solution; and 4) activity coefficients of all species are unity. We can then calculate the partial pressure of oxides as:



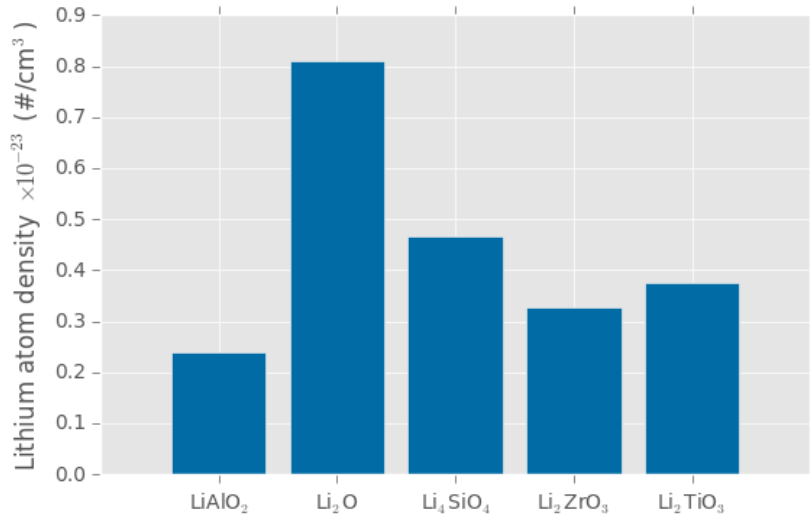


Figure 1.2: Lithium oxide is the only ceramic with lithium density sufficiently high to potentially operate without a neutron multiplier. All other ternary oxides have comparable lithium densities.

and

$$p(T_2O) = X_M X^2 K_p \quad (1.4)$$

where $p(T_2O)$ is the partial pressure of T_2O , X is the mole fraction of LiOT , and X_M is the mole fraction of the binary metal oxide (e.g. TiO_2).

As neutrons transmute lithium from the ceramic, the stoichiometry of the material will begin to change. There is great uncertainty in the activity of lithium-depleted species. The lithium depleted species may not exist in the simple metal oxide form (e.g. Al_2O_3) but most probably another ternary compound (e.g. LiAl_5O_8). In the examples of lithium aluminite, LiAl_5O_8 is more stable than LiAl_2O_3 and therefore free energy changes and k_p values for reactions may be overestimated. Moreover, the composition of the breeding material continuously changes during operation of the blanket because of lithium burn-up. Because tritium is being removed from the blanket, the mole fraction of LiOT will reach a constant value. However, the concentration of other species (metal oxides) will continuously increase.

Although there is considerable uncertainty in many of the terms of Equation (1.3), approximations can be made for many of the candidate ceramics. Equilibrium tritium concentrations in solid ceramic breeders for a T_2O partial pressure of 1.3 Pa were calculated by Clemmer and his results are reproduced in Figure 1.3. [11] From estimates of solubility shown in Figure 1.3, it is immediately apparent that all the

ternary oxides have significantly lower tritium “solubilities” than Li_2O . In spite of the promising feature of Li_2O being capable of existing without a neutron multiplier due to its high lithium density, the tritium inventory of the material may be unacceptably high.

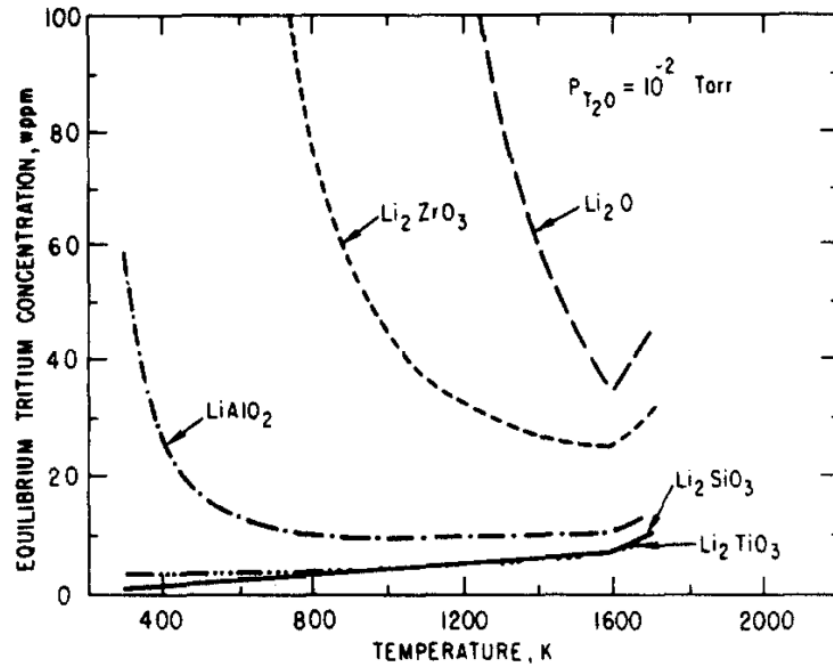


Figure 1.3: Calculated equilibrium tritium concentrations in candidate solid breeding materials at $P_{T_2O} = 1.3 \text{ Pa}$.

1.1.3 Tritium Release and Recovery

Tritium recovery from solid tritium-breeding materials is a key factor in establishing the viability of the solid-breeder concept. Designs of solid breeders have tritium removed with a purge gas (primarily helium) flowing through the open porosity of packed beds of lithium ceramics. The feasibility of the solid breeder concept is based on the capability of tritium to readily transport from the solid ceramic into the purge gas. Tritium release is a function of grain size, microstructure, and open/closed porosity. To understand the capability of tritium removal, five mechanistic steps are identified for bred tritium to be recovered (visualized in Figure 1.4). The steps follow as

1. bulk diffusion,

2. grain boundary migration,
3. desorption of tritium (T_2O),
4. percolation of tritium through pores internal to the solid ceramic toward the flowing purge gas,
5. convective mass transfer out of the blanket via purge channels.

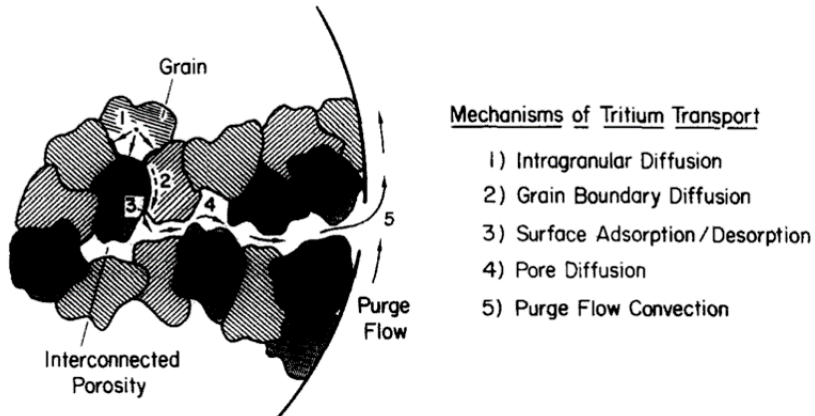


Figure 1.4: Mechanistic steps of tritium transport through ceramic materials into the purge gas for removal.

Bulk diffusion of tritium is considered to be a significant contributor to tritium inventory. For spherical particles of radius r_p , assuming zero surface concentration, the tritium inventory T is given by

$$T = \frac{1}{15} \dot{T} \frac{r_p^2}{D} \quad (1.5)$$

where \dot{T} is the tritium generation rate and D is diffusivity of tritium in the ceramic. It is significant to note that the tritium inventory is a function of the square of the particle size. Thus it is clear that: (i) small grain sizes are required for minimum tritium inventory and (ii) grains should not significantly grow during the lifetime of a reactor blanket. Diffusivity values of tritium in ceramics are extremely scarce and with much uncertainty. Kinetic experiments of post-irradiation tritium release from several candidate breeders have been performed. The kinetics in the experiments are non-steady-state and the diffusivity is given by

$$D = 0.16 \frac{r_p^2}{\tau} \quad (1.6)$$

where τ is the mean residence time, defined as the time required to extract 87.4% of the tritium. Combining Equation (1.5) and Equation (1.6) eliminates diffusivity and radius (with large variation between particles and grains), yielding:

$$T = 0.42\dot{T}\tau \quad (1.7)$$

We can then estimate the diffusive inventory in a blanket based on the readily measured residence time, τ . It must be kept in mind that the particular micro-structure of the ceramics measured in kinetic experiments must correspond to the micro-structure of the material in the blanket in order for the diffusivity predictions to hold. In other words, residence times of 1 mm Li_2TiO_3 with average grain sizes of $\mu = 1 \text{ m}$ are utterly inappropriate to calculate tritium diffusion in 0.5 mm pebbles of Li_4SiO_4 with average grain sizes of $\mu = 5 \text{ m}$, for example.

The tritium generation rate, \dot{T} is a function of the fusion reactor power output and blanket design. Assuming this value is known for a given blanket, residence times have been measured to be temperature dependent which is consistent with diffusion-controlled processes. Therefore, based on the present model, the range of operating limitations are defined on the low end where bulk diffusion is the rate-limiting step. A minimum temperature is defined as the temperature at which the tritium inventory exceeds 1 kg GW¹. The minimum temperatures for many candidate materials are shown (with slight variation between sources) in Figure 1.5. Minimum temperatures generally range from 300 up to 400 C.

As we saw from Equation (1.5), tritium inventory goes with the square of grain size and thus another operating limit on temperature arises. An upper limit of temperature is based on restructuring or grain growth in ceramics which can greatly affect the diffusive inventories. When ceramic materials are heated above their sintering temperature, generally in excess of $0.8T_{\text{melt}}$ (in absolute temperature), grains will grow. The effects of sintering at 1200 C over a number of hours is shown in Figure 1.6 (images courtesy of Yi-Hyun Park from NFRI). Grain growth, as witnessed in these images, must be avoided in operation.

Moreover, neutron radiation typically enhances sintering characteristics and lowers sintering temperatures; effects of radiation are expected to reduce the sintering temperature to $0.6T_{\text{melt}}$. [31] Maximum temperatures are thus set by sintering considerations. Candidate materials are compared in Figure 1.7. In general, keep in mind that acceptable candidate materials have their maximum temperature between 750 and 900 C.

As a consequence of the tritium inventory of solid breeder material, we are faced with a relatively narrow operational temperature to which solid breeder designers must adhere, roughly between 350 and 800 C. Thus to provide designers the ability to optimize breeder volumes for tritium breeding and subsequent tritium release, we must understand the important physics and phenomena dictating thermophysical properties and thermomechanical responses of pebble beds during operation

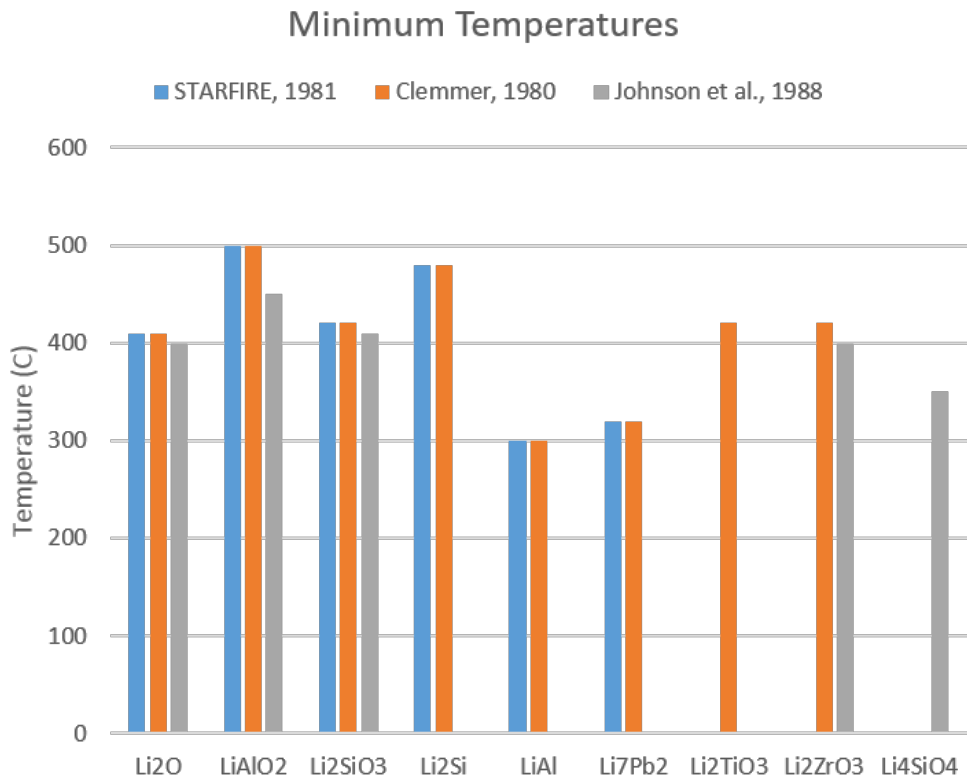


Figure 1.5: Minimum temperatures for various candidate materials (compiled from various sources) based on rate-limiting diffusion processes.

in a fusion reactor. Thermomechanical modeling of solid breeder pebble beds remains an important field in solid breeder research and much of Chapter 2 will focus on this topic.

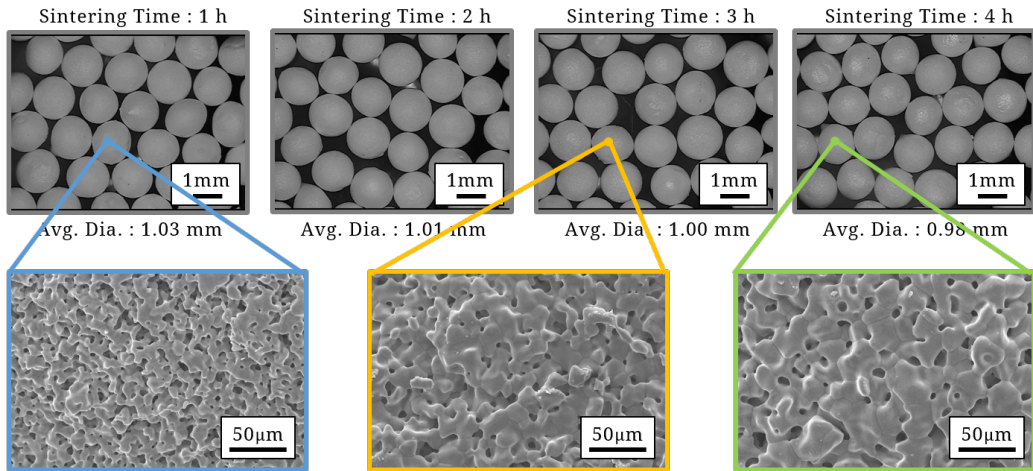


Figure 1.6: Maximum temperatures for various candidate materials (compiled from various sources) based on irradiated sintering temperatures ($0.6T_{\text{melt}}$).

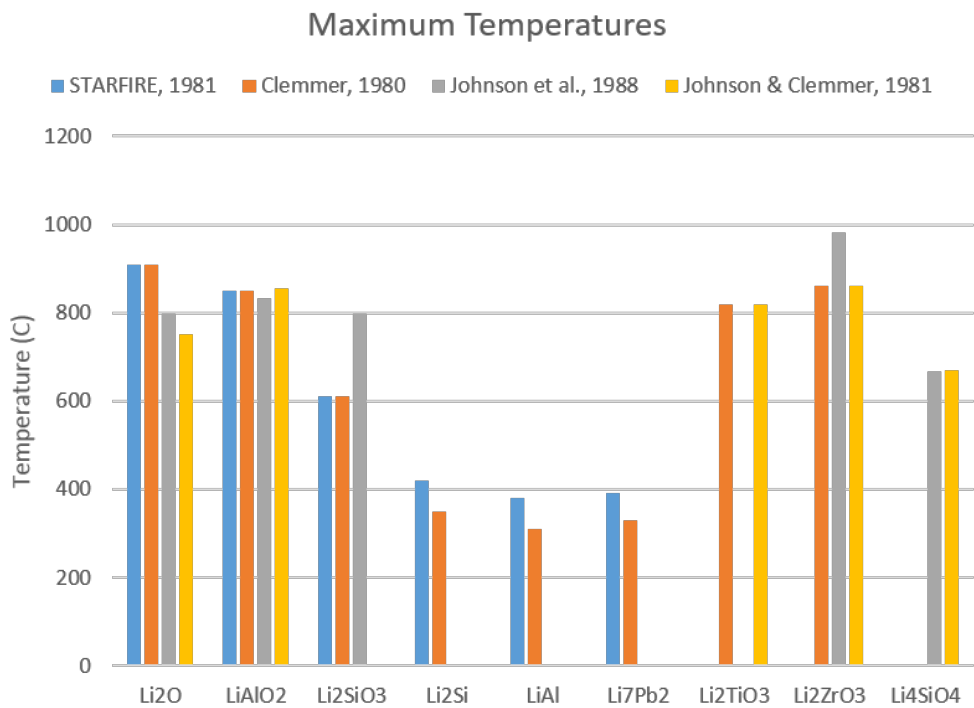


Figure 1.7: Maximum temperatures for various candidate materials (compiled from various sources) based on irradiated sintering temperatures ($0.6T_{\text{melt}}$).

1.1.4 Physical & Thermophysical Properties

The temperature window established for tritium release dictates the thermal characteristics of pebble beds become critically important to understand. Candidate ceramic materials is itself quite low, being reduced by porosity. Several candidate conductivities are given in Figure 1.8 assuming 80% theoretical density; Li_2TiO_3 has comparable conductivities with Li_4SiO_4 .

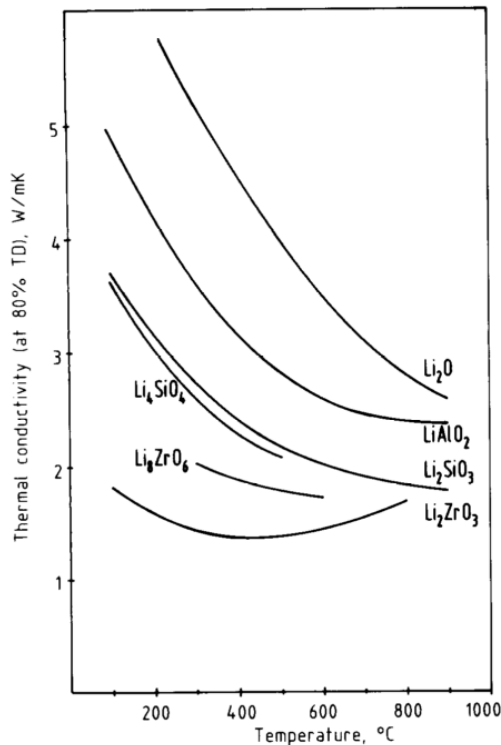


Figure 1.8: Solid conductivities of several ceramic materials, assuming 80% theoretical density.

Elastic modulii of material is a manifestation of atomic bond strength and can thus provide qualitative information on lattice defects. [33] In irradiation experiments of LiAlO_2 with a fluence of 10^{20} neutrons cm^{-2} , no change in Young's modulus was observed up to 400 C though approximately 10% reduction in Young's modulus was found at 600 C. At the same higher temperature, no change was found for Li_2O . Compressive strength was also measured for LiAlO_2 to be a relatively strong function of temperature (decreasing with increased temperature) but not irradiation, up to 2 at.% burn-up.

A comprehensive review of Li_2TiO_3 material properties can be found in Ref. [27]

Many properties of Li_4SiO_4 can be found in Ref. [18]

1.1.5 Compatibility

Compatibility studies have been carried out at several temperatures between various pairs of breeder and structural materials. [33] Li_5FeO_4 , Li_2CrO_2 , and $\text{Li}_2\text{Ni}_8\text{O}_{10}$ were common corrosion products (varying by structural material). Li_2O was seen to be most reactive; reaction rates for Li_4SiO_4 , Li_2ZrO_3 , and LiAlO_2 were much lower. However, in studies of Li_2O where the material was rigorously freed of moisture impurity, Li_2O was found to be inert to metals. Corrosion properties of Li_2O are therefore attributed to the presence of highly corrosive LiOH contamination happening in the presence of water with Li_2O . In general, reaction rates increase with increasing temperature and moisture content. [32] From compatibility point of view, ternary oxides such as Li_2TiO_3 and Li_4SiO_4 are more desirable.

Compatibility of ceramic materials with neutron multiplying materials is also necessary to understand. Interaction of ternary oxide ceramics with beryllium was found to be counter to expectations based on thermodynamics and seen to be negligible up to 650 C for Li_4SiO_4 , up to 700 C for LiAlO_2 and Li_2ZrO_3 , for durations up to 3000 hours. A beryllium oxide layer is assumed to form on the material surface, thereby protecting it from further oxidation. The SIBELIUS experiment studied the effect of neutron irradiation on the BeO layer. Data from SIBELIUS indicate the beryllium oxide layer appears to have some influence on the amount of tritium retained by the beryllium discs. The tritium release from the ceramics, on the other hand, is consistent with other tritium release measurements of the ceramic materials in the absence of beryllium and therefore appears to not be affected by adjacent beryllium. [35, 48]

Recently, advanced neutron multiplier material has been considered which overcomes some compatibility issues with pure beryllium. For example, beryllides (such as Be_{12}Ti) offer higher melting point, better compatibility than pure beryllium, significantly lower tritium inventory, and sufficiently high tritium breeding ratios. [34] Development of advanced materials continues to be a rich bed of research.

1.1.6 Radiation Effects

We have already discussed the anticipated effect of radiation on lowering predicted sintering temperatures of candidate ceramic materials. While in a fusion reactor, the ceramic materials will be subjected to high temperatures and changing material characteristics from the neutron environment. The neutron capture reaction of $n + {}^6\text{Li} \longrightarrow \text{T} + \text{He}$ produces significant lattice damage during irradiation. [31] Not only are two large gas atoms produced, one of which is not expected to be soluble in

the parent material, but also a lithium vacancy is produced. Several anticipated radiation damage mechanisms are:

- Displacement Damage
 - Vacancies
 - Loops, Clusters, etc.
 - Interstitials
- Reaction Products
 - Bubbles
 - Interstitials
 - Substitutional Defects
- Lithium Depletion
 - Vacancies
 - Oxygen Excess
 - Nonstoichiometry
- Microstructural
 - Sintering
 - Grain Growth
 - Microcracking

and the manifestation of these atomistic changes as microstructural damage must be evaluated with irradiation experiments.

In lithium ceramics there are a minimum of two sublattices composed of anions and cations. Creation of more defects on one sublattice than the other, for instance on the oxygen lattice, would lead to charge separation within the matrix. If sufficient defect mobility exists, the newly formed defects can annihilate or cluster, forming voids or precipitates within the crystal. Displacement damage to lattices is quantified with a value displacements per atom, dpa. In fusion reactors, solid breeder materials will receive substantial displacement damage from high energy neutrons of the plasma. Fusion neutrons that have been slowed (from interaction with neutron multiplication or structural materials) to lower energies will produce much less displacement damage.

Ceramic materials primarily conduct heat by phonon transport. Irradiation-induced vacancies act as phonon scattering centers and consequently thermal conductivity of ceramics is reduced under irradiation. [29] Fast neutron damage can

produce large populations of defects and thereby reduce room-temperature thermal conductivity of ceramics by orders of magnitude with doses ≤ 1 dpa. [51] Analysis of breeding blanket modules for ITER indicate a maximum expected neutron damage in steel to be about 3 dpa over a span of 20 years of operation. By comparison, dpa levels required for DEMO are greater than 70 dpa. [26] Reduced thermal conductivity due to fast neutron damage is a concern for blanket designers and this study is meant to address pebble bed thermal reactions to irradiated pebbles.

Neutron fluence in ITER is targeted to reach 0.3 MW yr m^2 . [1, 58] In terms of 14 MeV neutrons, this equates to a fluence of $4.22 \cdot 10^{24} \text{ n m}^2$. Kawamura *et al.* carried out irradiation experiments on Li_2TiO_3 pebble beds to detect changes in effective thermal diffusivity. They found a reduction in thermal diffusivity of 30% compared to unirradiated pebble beds at 400 C but report that no change in effective thermal conductivity is detectable up to thermal neutron fluence of $1 \cdot 10^{24} \text{ n m}^2$.

An experimental irradiation campaign has been carried out in Petten, Netherlands as part of the European program for development of HCPB blanket concept, a high fluence irradiation project, HICU (High neutron fluence Irradiation of pebble staCks for fUsion). The high fluence irradiation of lithium ceramics was meant to be up to DEMO-relevant values of 20 to 25 dpa, even with a neutron spectra not including 14.1 MeV . [28, 61] Temperatures in ceramic regions dropped during the experimental campaign, trailing somewhat the tritium production rate and lithium burn-up. On-line temperatures were measured during the year-long experiment, temperatures in ceramic pebble regions were measured between 600 K to 800 K . Similar to Kawamura *et al.*, a significant increase in temperatures as a result of decreased thermal conductivity was not witnessed. However, careful thermal characterizations of ceramic pebble beds under irradiation were not evaluated.

The experiment of Kawamura *et al.* reached neutron fluence of the same order of magnitude of a years operation in ITER though only with thermal neutrons. HICU matched much of the neutron energy spectrum, save for the highly energetic fusion neutrons. Both experiments did not detect significant reductions in thermal conductivity. The results are providential for ceramic breeder regions far from first walls. Nevertheless, damage from fast neutrons in near-wall regions remains a concern.

Helium generated in the solid breeder material during irradiation, owing to its inert nature, will have a much lower solubility in ceramics than tritium, since only interstitial positions are available. The lower solubility for helium will result in a lower permeability so that the rate of migration out of the lattice will be less. Moreover, low solubility will enhance bubble formation and swelling. Swelling can have significant negative consequences on the mechanical stability of ceramic pebbles.

A consequence of neutron capture is loss of lithium atoms from ceramic lattices. This loss creates either a lithium vacancy or a localized excess of oxygen, *i.e.* oxygen interstitials. Since tritium ions are created during the neutron capture of a lithium

ion, the overall electrostatic equilibrium of the crystal is maintained. When the tritium ions are subsequently released to the purge gas, it necessarily follows that the oxygen ions must also be released in order to avoid a charge buildup in a single valency system. If multivalent ions (*e.g.* Fe^{+2} , Fe^{+3}) are present, then a change in oxidation states would balance the charge of the excess oxygen. From this point of view, it is natural that we observe tritium released as T_2O in Li_2O systems rather than as a hydrocarbon or T_2 . [31]

As mentioned previously, when lithium depletion (or lithium burn-up) occurs to a significant extent (around 5%), the resultant nonstoichiometry in ternary oxides could establish, rather than single-phase conditions. For example, under irradiation and lithium burn-up, Li_4SiO_4 ceramics would develop an excess of silica and the melting point of 1300 C would drop to a eutectic temperature of 1024 C. Such a reduction in melt temperature would have significant impact on sintering and tritium inventory in the solid breeders. [31]

Lastly, an attractive feature of fusion energy is its ability to operate in an environmentally benign way. This feature must not be lost during the choice of material candidates in the development of tritium breeding technology. One acceptable guideline put forth calls for all materials to meet requirements for near-surface burial as radioactive waste. [49] Long-lived daughter nuclides of ternary oxides should be avoided during primary candidate considerations. From this perspective, Li_2TiO_3 and Li_4SiO_4 are more attractive than Li_2ZrO_3 , due to long-term radioactive characteristics of the latter.

This list of irradiation effects is by no means complete and irradiation experiments are still ongoing. [57] Moreover, experiments that can recreate fusion neutron sources are necessary steps towards realizing solid breeder technology and are under development. [2]

1.1.7 Fabrication

One last point to discuss on ceramic materials before moving on to a discussion of neutron multipliers concerns fabrication. Candidate ceramic material feasibility is in part dependent on the fabrication price and ability to scale to industrial output quantities. While this is an important point for realization of solid breeders, it will not be discussed in detail here. van der Laan *et al.* [57] and Johnson *et al.* [32] provide thorough descriptions and discussions for various fabrication techniques.

1.2 Neutron Multiplication in Solid Breeders

Because neutron multiplying material is a necessity for all ternary oxides, we will discuss some of the important aspects of neutron multiplication materials. Beryl-

lum is identified as the most suitable material for neutron multiplication in solid breeders. The common reaction of ^9Be is:



with a threshold energy of about 1.8 MeV. The following reaction also has small probability of occurrence



with a threshold energy of about 0.7 MeV. ${}^6\text{He}$ is unstable and undergoes β^- decay into ${}^6\text{Li}$ (with 99.99% probability and a half life of only about 800 ms), which itself may interact with high energy neutrons to form tritium inside the neutron multiplier.



While the $(n, 2n)$ reaction is much more likely to occur, the (n, α) reaction is non-negligible. Cross-sections for the two reactions are given in Figure 1.9. The tritium-producing reactions must be considered from a safety stand-point of tritium retention in beryllium.

The melting temperature of natural beryllium is 1250 C, advantageous for solid form of neutron multiplier with solid tritium breeder. Aside from pure beryllium, other options have been considered. Beryllium will also exist as a pebble bed.

A short list of salient points:

- Be incompatibility with structure steel, forming FeBe_{13}
- Be reaction with water forming BeO ($\text{Be} + \text{H}_2\text{O} \longrightarrow \text{BeO} + \text{H}_2$)
- Be reaction with oxygen forming BeO ($2 \text{Be} + \text{O}_2 \longrightarrow 2 \text{BeO}$)
 - BeO has excellent compatibility with structural steel
 - BeO is a carcinogen, causes beryllium disease if inhaled
- Diffusional release of T from irradiated beryllium is very slow

As discussed previously, an alternative to pure beryllium that has been receiving much attention lately is the beryllide of Be_{12}Ti . The advantages of this material include: [34]

- more compatible with steel than Be

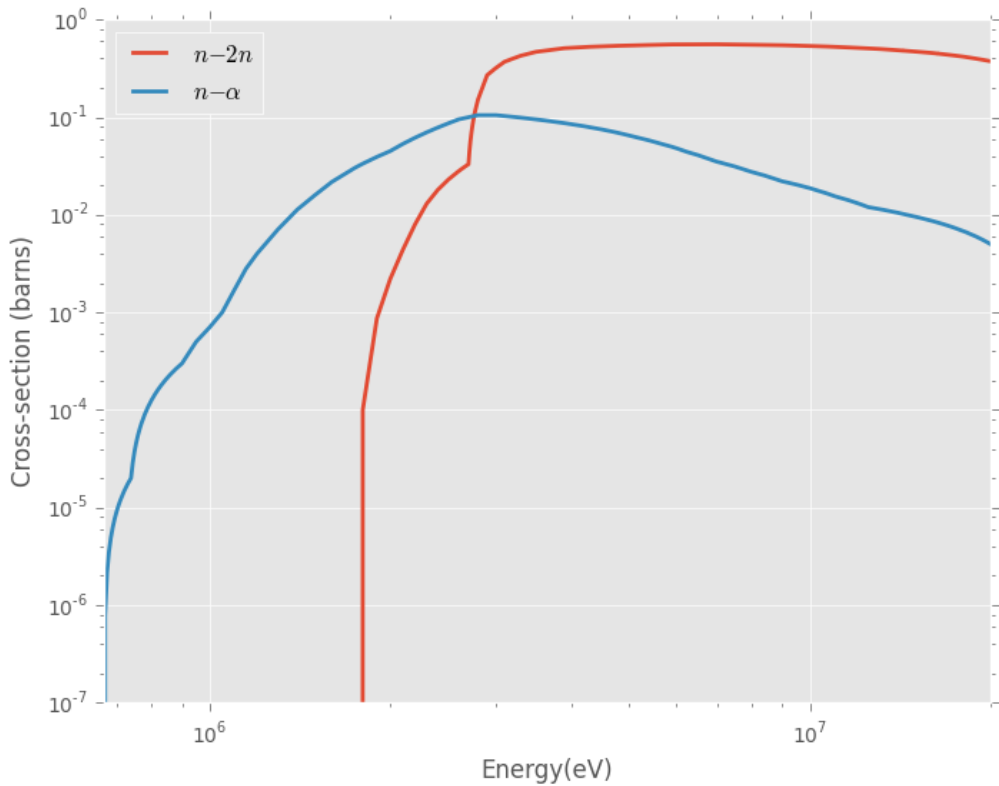


Figure 1.9: Beryllium cross-section for $n,2n$ and n,α (ENDF data from <http://atom.kaeri.re.kr/>).

- less swelling than Be
- tritium inventory of beryllide is significantly lower than Be
- high Be density maintains neutron multiplication characteristics (sufficiently high tritium breeding ratio)

Lastly, we must bear in mind limited abundance of Be on Earth (remember Homework set). Thus we must be economical in our consumption of beryllium for neutron multiplication in fusion reactors.

Chapter 2

Introduction to Solid Breeder Analysis

The solid breeder concept with sphere-pac beds satisfies the requirements of a breeder unit: transmute lithium into tritium, act as shield to other sensitive equipment and personnel, and convert energy into extractable heat for electricity production. Common features of pebble bed designs are:

1. Always separately cooled with (with *e.g.* helium or water)
2. Necessity of neutron multiplication
3. Surrounded by a structure of reduced-activation ferritic steel

In a typical solid breeder module, the module is subdivided into several alternating layers of neutron multiplication material (generally beryllium) and tritium breeding material. The layers are separated by steel plates with internal channels for coolant. A conceptual design of the Japanese solid breeder for ITER is shown in Figure 2.1.

Pebble bed forms of tritium breeding volumes have several advantages which include: large surface area to volume, ease of assembly of granular materials into complex geometries, bred tritium can be readily removed with large open porosity between pebbles, and temperature gradients across any single pebble are small enough to avoid damage from thermal stress.

In this chapter, we will review the need for accurate thermal management in solid breeders. We will then present engineering analysis considerations for the interstitial purge gas and fluid coolant as they are necessary for solid breeder design. Following that we will introduce phenomenological models of effective material properties for packed beds, experiments from which constitutive equations can be derived, and solid breeder modeling tools.

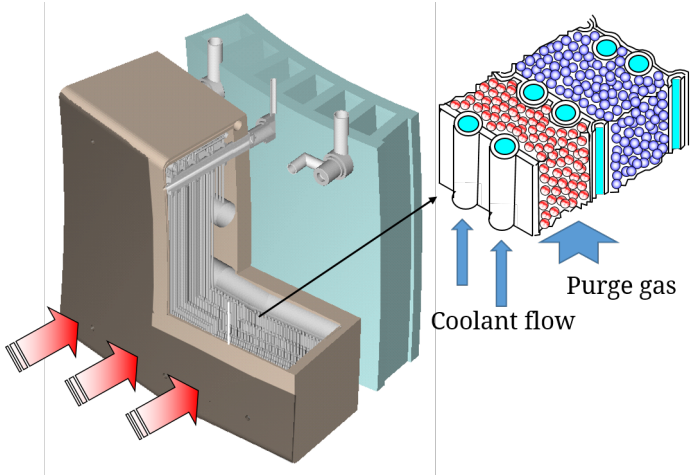


Figure 2.1: Sketch of a typical unit of a pebble bed tritium breeding zone. The pebble bed is cooled with contact to the containing structure.

2.1 Solid Breeder Thermal Management and Imposed Temperature Window

Tritium breeding blankets will experience high volumetric heating as deposited by high-energy neutrons that are carrying away approximately 80% of the fusion reaction energy in addition to heating from secondary γ rays. Heat deposited in breeders must be transported through pebble bed regions into the walls of containing structures, then ultimately into the coolant gas. Heat deposited into pebble beds will transfer *via* inter-particle contact conduction, inter-particle radiation, and convection with the helium purge gas. At the interface with the structural material, similar modes of heat transfer are present: particle-wall contact conduction, particle-wall radiation, and communication *via* helium purge gas convection. There exists a coupling between mechanical forces acting upon beds and their heat transport capabilities and we must consequently understand packing structures in order to understand heat transfer.

The structure of packed beds can be considered as a metastable configuration that will last indefinitely unless acted upon by an external perturbation such as vibration or compressive pressure. [30] The ability of a metastable configuration to resist perturbations can, in some way, be quantified by the initial packing fraction. For more compliant beds (lower packing fractions), stresses from thermal expansion can cause significant rearrangement of the packing structure which is not recoverable after stress removal. This phenomena has been observed in numerous experiments as so-called plastic rearrangement of pebble beds. [42, 43, 64] Plastic-

ity of beds may have significant consequences for the ability of the pebble bed to maintain contact with the containing structure and routes for heat out of the bed due to gap formation between pebble volumes and coolant walls. As the pebbles heat under the nuclear load, thermal expansion of the pebbles in the packed volume will be contained by cooler structural material. Confined expansion will give rise to increased contact pressure between pebbles. Moreover, increased pressure between pebbles can cause, among other effects, brittle pebbles to fragment.

Some amount of restructuring of pebble beds (and internal contact force networks) are also likely to occur from crushing/cracking of individual pebbles, or the effects of inter-pebble sintering and creep arising from the high-temperature, high-stress environment in a breeder unit. Contact conduction in beds, intimately linked to the packing structure, will be impacted during operation of ceramic pebble beds in fusion reactors. Concurrently, interaction of the slow-moving purge gas with tightly packed pebble beds is an additional route of heat transfer that must be understood. Thus, heat transfer in pebble beds is quite different from standard solid materials and requires specialized modeling of the synergistic physics. Knowledge and characterization of thermal transport must anticipate changes to the heat transfer capabilities and predict temperature profiles for pebble bed packing structures that will emerge after initially-packed pebble beds react to prolonged exposure to fusion reactor environments.

We saw earlier that tritium inventory requirements impose a relatively narrow operational temperature window on lithium ceramic pebble beds. Given the high power densities in fusion power reactors, it is therefore necessary to have accurate knowledge of ceramic pebble bed thermomechanical behavior and comprehensive characterization; reliable models of heat transfer in solid breeders are critical for solid breeder designs. In addition, due to the complicated nature of granular materials, heat transfer in these solid breeder volumes remains transient during fusion operation.

2.2 Purge Gas and Coolant Flow

All heat deposited into the ceramic pebble beds is conducted towards the structure and into coolant. Coolant proceeds out of the tritium breeding module and into a standard electricity production cycle where heat is extracted. After tritium is generated inside the ceramic, the bred tritium is ultimately carried away by a low-pressure, slow moving purge gas (primarily helium) and extracted in a closed loop for fuel. A sketch of a generic volume of ceramic pebble bed is given in Figure 2.2

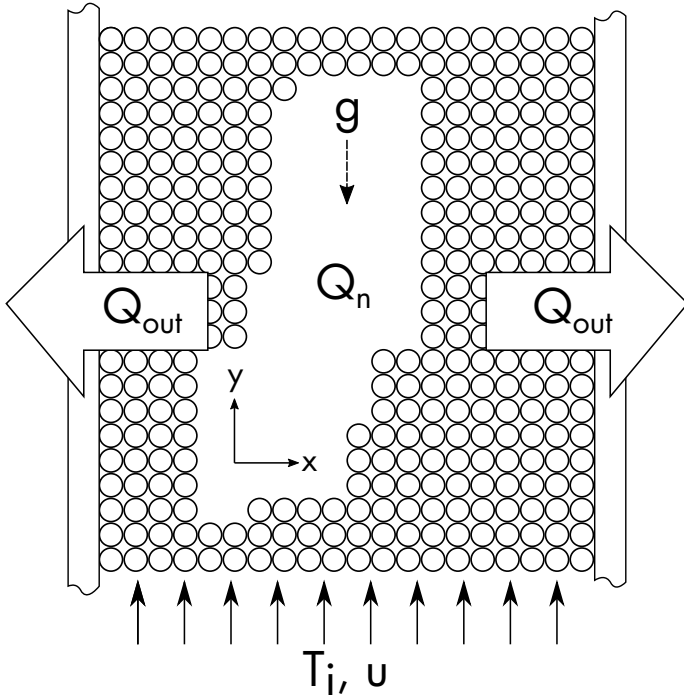


Figure 2.2: Sketch of a typical unit of a pebble bed tritium breeding zone. The pebble bed is cooled with contact to the containing structure.

2.2.1 Purge Gas

The purge gas composition is generally helium with small amounts of hydrogen which promotes tritium release from ceramics. Flow rates of purge gas are kept low to minimize the pressure drop across tightly packed pebble beds.

Pressure drop (per unit length) for the purge gas can be calculated based on the Kozeny-Carman correlation; derived for packed beds at the close-packed limit,

$$\frac{\Delta p}{L} = \frac{180 \bar{U} \mu}{d_p^2} \frac{(1 - \epsilon)^2}{\epsilon^3} \quad (2.1)$$

where μ is the viscosity, ϵ is the void fraction, d_p is the particle diameter (assuming spherical) and \bar{U} is the superficial velocity of the fluid in the packed bed.

Carman points out the limitations of applicability of the Kozeny-Carman (KC) equation: built into the equation is the assumption that the range of pore size and shape is fairly isotropic and similarly the tortuosity through the packed bed is relatively uniform. Pressure drop as a function of Reynolds number for 1 mm particles in a packing fraction of $\phi = 1 - \epsilon = 0.645$ in helium at 600 C is given in Figure 2.3.

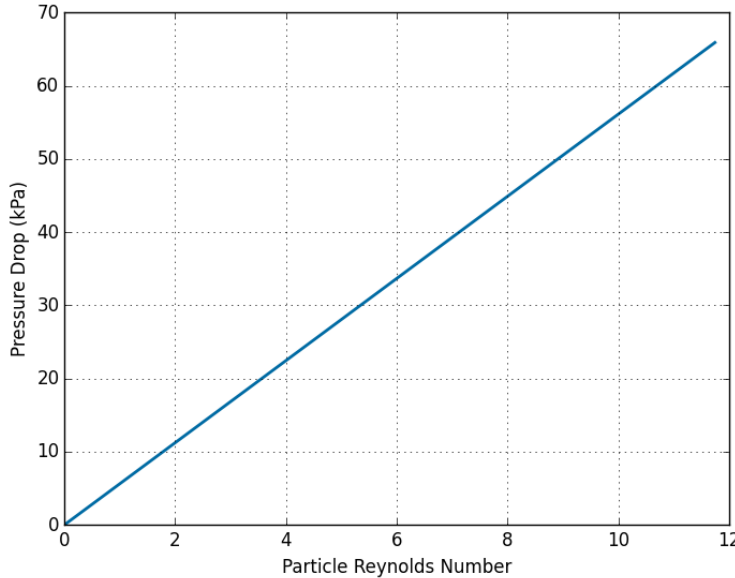


Figure 2.3: Kozen-Carman pressure drop increases linearly with particle Reynolds number.

Tritium permeation from the purge gas through piping is a safety concern for solid breeders. Tritium extraction and permeation will be covered in another lecture of this class.

2.2.2 Coolant

The function of coolant is not only to maintain ceramic breeder volumes within specified temperature windows and keep structural materials under their operable limits, but also to extract high-quality heat for power generation. Current tritium breeding designs call for a high pressure helium, approximately 8 MPa. Inlet temperatures of coolant are sufficiently high to maintain the minimum temperature of breeder volumes, coolant inlets are approximately 300 C. The coolant is run such that the outlet is held around 500 C; obeying concerns for structural integrity of the steel container that happen around 600 C.

Analysis of the coolant is nothing exotic. We can apply standard engineering practices of heat transfer in a fluid duct such as the Dittus-Boelter equation for obtaining Nusselt number,

$$Nu_D = 0.023 Re_D^{4/5} Pr^{0.3} \quad (2.2)$$

where the equation is valid for $\text{Re} \geq 10000$ and the Nusselt and Reynolds numbers are based on the hydraulic diameter of the duct.

Lastly, one special consideration for the coolant are the safety issues of high pressure coolant stressing the structure or chemically reacting (or transporting tritium) during a breach. These concerns are specific to each tritium breeding volume and are often modeled before licensing is allowed for designs.

2.3 Phenomenological Properties of Packed Beds

One approach to studying heat transfer granular material is to treat the packed bed as a fictitious continuous media. Many experiments have been carried out for developing phenomenological models of effective material properties. In this approach, heat transport in pebble beds is often characterized with an effective thermal conductivity, k_{eff} , and interface heat conductance. Many models have shown their ability to accurately predict the temperature profiles for pebble beds under specific operating conditions. We begin with a review of k_{eff} correlations.

2.3.1 Empirical Models for Heat Transfer Packed Beds

Deissler and Boegli, in 1958, proposed upper and lower bounds of effective thermal conductivity, k_{eff} , in two-phase granular media to be given by alternating layers of the two phases arranged in parallel or series, respectively [12]. In the case of parallel layers, effective conductivity, normalized by fluid conductivity, is

$$\frac{k_e}{k_f} = \epsilon + (1 - \epsilon)\kappa \quad (2.3)$$

where k_f is the fluid conductivity, $\kappa = k_s/k_f$ is the ratio of solid to fluid conductivity, and ϵ is the void fraction in the porous media. Similarly, the minimum effective conductivity is found in a serial layering of the solid and fluid phases,

$$\frac{k_e}{k_f} = \frac{1}{\epsilon + (1 - \epsilon)/\kappa} \quad (2.4)$$

Equations (2.3) and (2.4) act as theoretical upper and lower limits to true effective thermal conductivities of real material.

One of the most widely-used correlations was put forth by Zehner and Schlunder in 1970 [62, 63]. They considered a cylindrically-shaped unit cell and made the analogy between heat and mass transfer to derive an empirical fit to data in the bulk of two-phase porous media. The Zehner-Schlunder (ZS) correlation is

$$\frac{k_e}{k_f} = \left(1 - \sqrt{1 - \epsilon}\right) + \frac{2\sqrt{1 - \epsilon}}{1 - B/\kappa} \left[\frac{(1 - 1/\kappa)B}{(1 - B/\kappa)^2} \ln\left(\frac{\kappa}{B}\right) - \frac{B + 1}{2} - \frac{B - 1}{1 - B/\kappa} \right] \quad (2.5)$$

where B is a deformation parameter related to porosity as

$$B = 1.25 \left(\frac{1 - \epsilon}{\epsilon} \right)^{1.11} \quad (2.6)$$

Over the years, many other correlations have been developed for predicting effective conductivity of packed beds. Some focus on conditions of higher porosity, consider radiation effects, or situations of large κ . A number of correlations have been plotted together along with the three presented here; given in Figure 2.4. Plotted on the figure is also a compilation of experimental data from many sources (reproduced from Ref. [55]) and recent COMET data recorded for graphite material at UCLA.

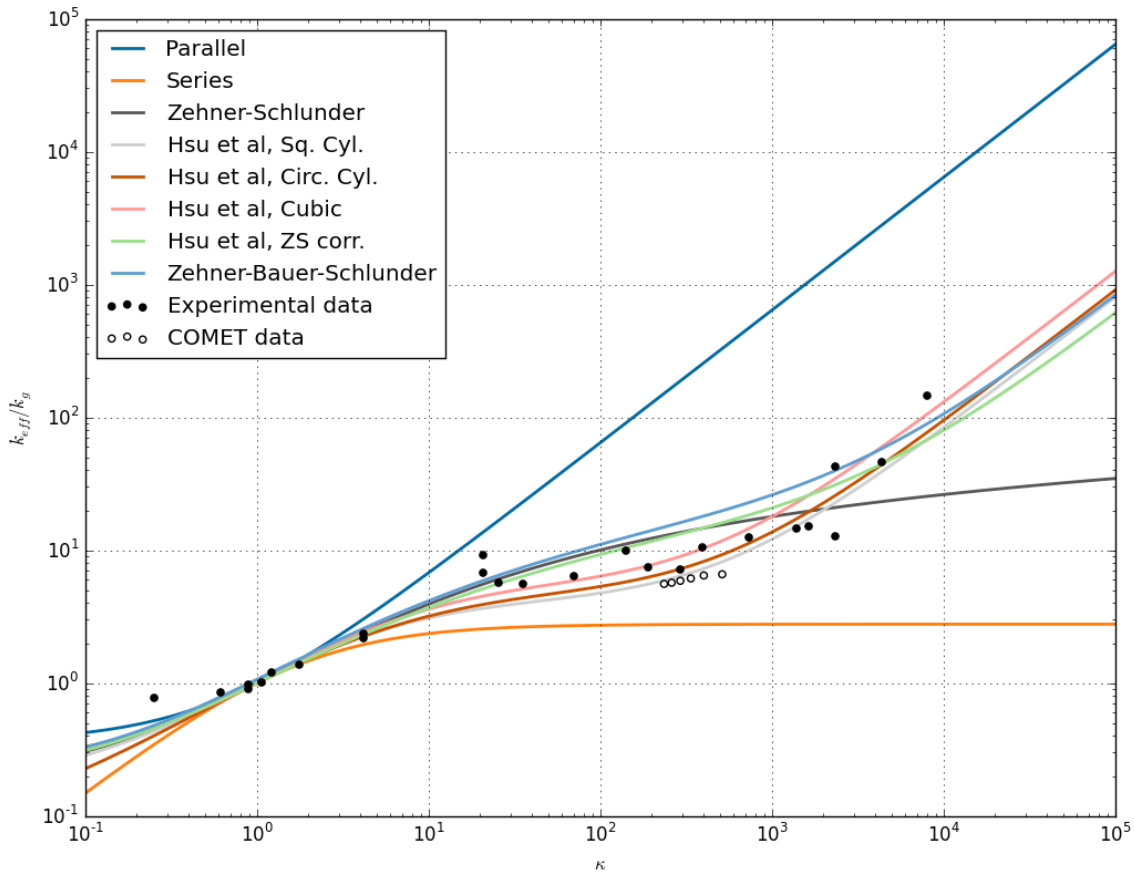


Figure 2.4: Comparison of COMET data on IG11 graphite, k_{eff} correlations, and experimental data. Data compiled by [55] from many sources and measured data at UCLA.

2.3.2 Experimental Measurements of Lithium Ceramics

Effective conductivities have been measured for several candidate ceramics. A reliable technique for measuring conductivity in packed beds is with a hot-wire technique; the technique is thoroughly described in ASTM standard C1113/C1113M document. Briefly, hot-wire measurements are done by raising the temperature of a pebble bed up to a background value (the reported value of $k_{\text{eff}}(T)$), then pulsing an electric current through a wire embedded in the bed. The pulse of heat on the wire decays as energy is conducted into the pebble bed. The rate of decay provides information on effective thermal diffusivity and thermal conductivity of the packed bed. A sketch of a hot-wire assembly and the former setup at JAEA is shown in Figure 2.5.

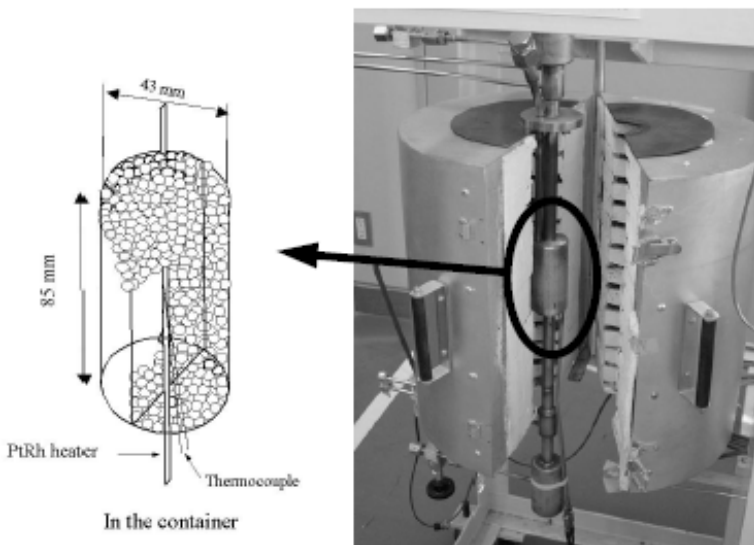
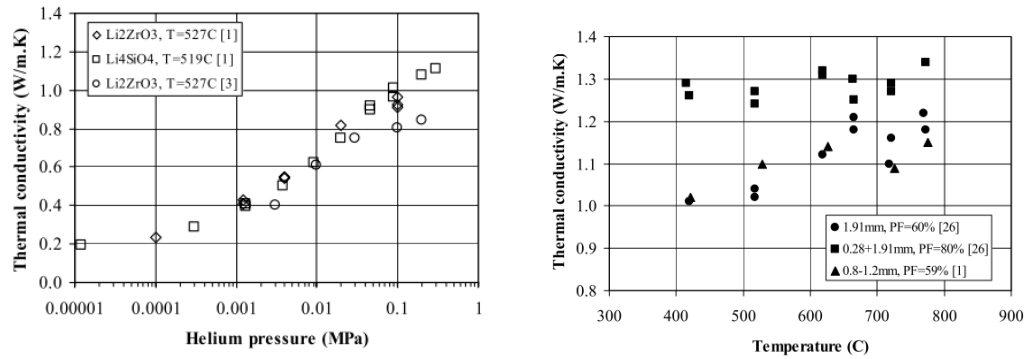


Figure 2.5: Schematic of hot wire embedded in a pebble bed and the realization in JAEA's lab (right).

Many experiments have been run to measure the effective thermal conductivity of a volume of ceramic pebbles. In Figure 2.6, the effective conductivity is seen to be strongly affected by the interstitial gas but weakly affected by the mechanical loads on the bed. The main conclusions to bear in mind from Figure 2.6 are that: 1) the interstitial gas is an important transporter of heat in the bed and 2) the effective thermal conductivity of the pebble bed is low and will limit the size of the ceramic pebble bed volume to satisfy the temperature window imposed on ceramic

breeders.



(a) Effective conductivity of ceramic pebble beds is dependent on the pressure below the Knudsen limit.
(b) The effective conductivity of pebble beds is weakly dependent on external mechanical pressure.

Figure 2.6: Effective conductivity of lithium ceramics. Results from Ref. [4]

Measurements for Li₄SiO₄ and Li₂TiO₃ are given in Figure 2.7 for different interstitial gases and packed bed temperatures. In a stagnant helium environment, the effective conductivity values for both materials fall to around 1 W m⁻¹ K⁻¹.

The coefficient of thermal expansion for a packed bed is also measured for candidate breeder materials. [52] The average thermal expansion coefficient for Li₂TiO₃ pebble beds is given in Figure 2.8; the measured values were approximately 78% of the value of bulk material under the same conditions studied for beds.

However, the accuracy of the model predictions often degrade as soon as a pebble bed's granular material, grain radii distributions, or operating conditions vary from the experimentally studied packed beds. In addition, propensity for creep, crushing, and inter-particle sintering of ceramic materials alter the packing structure in ways not currently predictable with the effective material characterizations. Furthermore, effective conductivity models that consider interstitial gas often assume the gas is stagnant. Much current study in the ceramic breeder field has been on developing more accurate and robust models of heat transfer in packed beds and their unique associated phenomena when employed in fusion reactors.

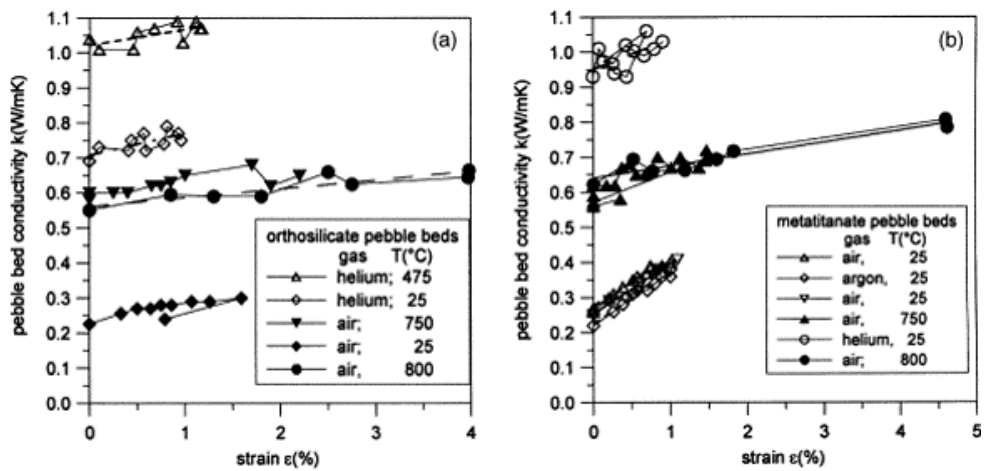


Figure 2.7: Effective conductivity of Li_4SiO_4 and Li_2TiO_3 .

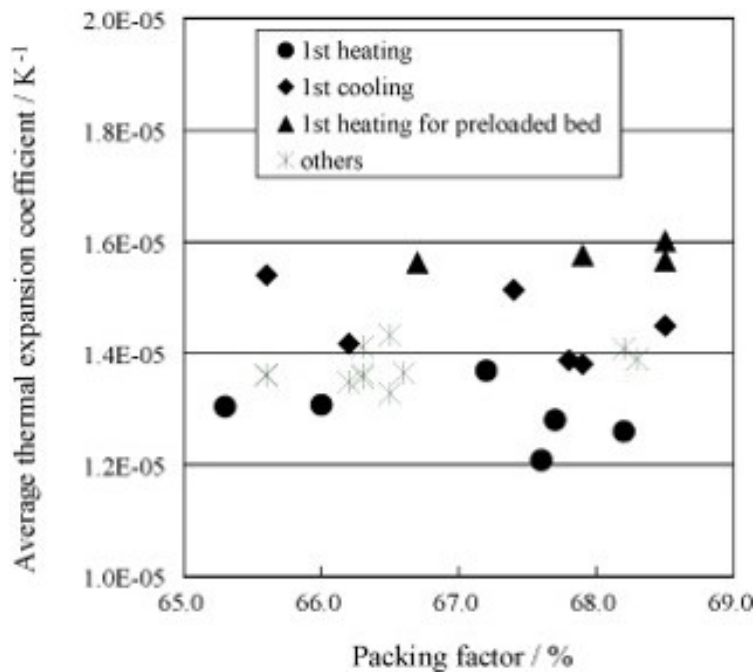


Figure 2.8: Effective thermal expansion of Li_2TiO_3 pebble beds is approximately 78% that of the solid material.

2.3.3 Thermo-mechanical Interactions

Reimann et al. have conducted an extensive experimental study of stress-strain relations of ceramic breeder pebble beds using an oedometric test apparatus [41, 43, 44, 46, 47]. The most significant macroscopic experimental phenomena witnessed in pebble beds is an irreversible plastic strain when load is removed, a non-linear elasticity, a pressure-dependent plasticity, and volumetric creep. A particularly noticeable feature, clearly demonstrated in Figure 2.9, is the reduced amount of irreversible strain when subjected to additional loading cycles after the first unloading. This may suggest the existence of a semi-equilibrium packing state in the pebble bed which can be reached after applying a pre-load to account for the large strain in the first cycle of a pebble bed. This semi-equilibrium packing state is a feature which may be advantageous for use in a fusion reactor.

To study temperature effects in Reimann's studies, beds are freely heated to desired working temperatures before pressure load is applied. Under the same loading condition, beds behave much softer at higher temperatures. The bed stiffens as the pressure increases. An illustration of this phenomenon is presented in Figure 2.10 for a lithium orthosilicate pebble bed between 50 C to 850 C. At higher temperatures (such as > 650 C), a creep-like behavior becomes apparent. Creep behavior allows the pebble bed to relax and sustain higher stresses, however at elevated temperatures we must keep in mind issues of surface sintering of pebbles. The data was used to correlate creep rate as a function of temperature, stress, and time for both lithium orthosilicate, lithium metatitanate, and beryllium pebble beds [9, 45, 47].

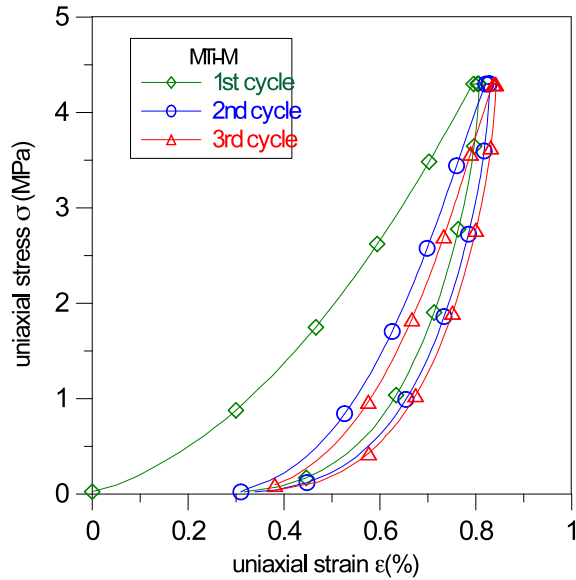


Figure 2.9: Example of uniaxial compression testing results for lithium metatitanate pebble bed [56].

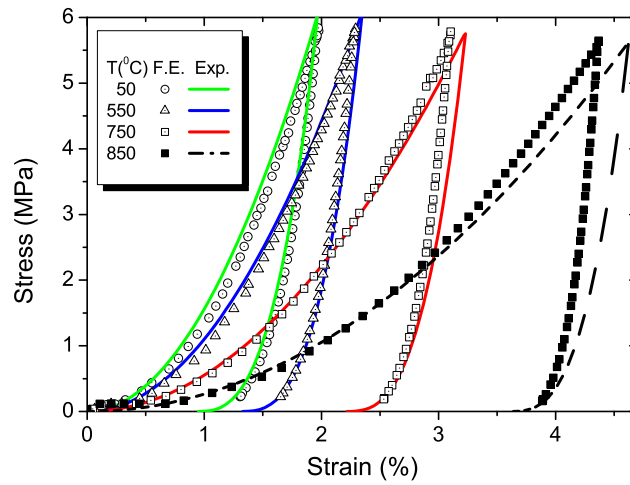


Figure 2.10: Example of uniaxial compression testing results compared with predictions from material constitutive equations for lithium orthosilicate pebble beds at different temperatures [22].

2.3.4 Post-irradiation Experiments

The pebble bed assemblies (PBA) experiment is designed to study the effect of neutron irradiation on the thermomechanical behavior of a ceramic breeder pebble-bed under DEMO representative thermomechanical loads [39]. This was accomplished *via* analysis of changes of the in-pile temperature profiles during irradiation as well as from the post irradiation examination of the pebble bed in the Hot Cells. Within the assemblies, there are four test elements; each resembling a small-scale mock-up of a HCPB TBM with a ceramic breeder pebble bed sandwiched between two beryllium pebble beds. Before irradiation, the beds are pre-compacted with a compressive load of 3 MPa to ensure good settling and contact.

FEM analysis was performed to study pre-compaction procedures. During progressive irradiation, temperatures are recorded at several locations in the ceramic breeder bed as well as other critical positions. Reviewing the recorded temperature data, when comparing the temperature in the center of the ceramic breeder pebble bed during later cycles and earlier cycles there appears to be a decrease in temperature for the exact same environmental conditions. Changes in the pebble beds and their characteristics are examined both in-pile by neutron radiography and out-of-pile by e.g. SEM during post-irradiation examination (PIE). The estimated bed height reduction from neutron radiographies over the course of the irradiation has shown 3% of creep compaction.

A pebble bed experiencing creep compaction is both becoming more dense as well seeing more-developed inter-pebble conduction paths. The effective thermal conductivity for a creep-compacted ceramic pebble bed is thus expected to be higher than a standard ceramic pebble bed. This phenomenon results in lower temperature gradients and a lower overall temperature magnitude, which is precisely what was observed in the experiment over the course of the cycling.

During PIE, various microscopy preparation techniques are used to study the deformation state of the pebble beds (signs of creep compaction and sintering), formation of gas gaps between the pebble beds and structural materials, and the interaction layers between eurofer-ceramic and eurofer-beryllium.

Figure 2.11 shows the cross-section of Li_2TiO_3 pebbles (left) and Li_4SiO_4 pebbles (right) post irradiation. Evident in the images is sintering of the lithium titanite and significant fracturing of the lithium orthosilicate pebbles. Importantly, however, it must be noted that the pebble beds performed reliably in spite of the changes displayed in these images. [39]

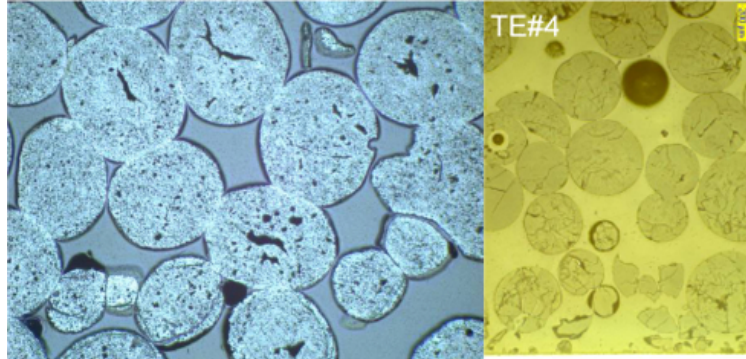


Figure 2.11: Notable features of irradiated Li_2TiO_3 and Li_4SiO_4 pebble beds from PBACitemagielsen2011. (Left) Demonstration of significant sintering of Li_2TiO_3 pebbles with no fracturing; the visible cracks originated from production and handling. (Right) Demonstration of cracking of Li_4SiO_4 pebbles.

2.4 Continuum Modeling of Packed Beds

When we consider beds of granular material from the standpoint of engineering continuum mechanics, packed beds cannot be adequately described by traditional models of either solids or liquids alone. Under compression, a packed bed responds like a solid with non-linear elasticity and a plasticity that is history-dependent. At the same time, the packed bed can obviously not support any tensile pressure and will often behave as an extremely viscous liquid as it may fill in voids under just the force of gravity. Nevertheless, phenomenological models, derived from the volumes of collected data (such as the data described in the above sections), have been developed, using effective material properties for the ceramic pebble bed, that describe the pebble beds in an Eulerian manner that provide reliable information on the initial states of breeder volumes in the fusion reactor environment and allow reasonable design predictions of the thermomechanics of the breeding blanket.

In spite of the shortcomings of a continuum approach, it is the only option which currently allows treatment of the pebble beds with standard finite element modeling (FEM) that can be scaled up to the breeder system. To employ FEM, mathematical models written in terms of average quantities and containing effective parameters are used. These models deduce a set of constitutive equations to be implemented in the framework of a finite element code. There are two major variants of phenomenological modeling approaches developed among institutions, including: (1) A non-linear elastic model and a modified Drucker-Prager-Cap theory for plastic strain [19, 21]; and (2) A hyper-porous non-linear elastic model and a Gurson model for the plastic model [13–15]. Another approach was taken by Ref. [19]

wherein the authors employed two different elasticity laws for the loading and unloading branches. Alongside the development of the modeling techniques, several large scale pebble bed thermomechanics experiments were conducted. These experiments were intended to reveal the underlined thermomechanical characteristics of ceramic breeder pebble beds, and provide data for benchmarking the developed models. The vast amount of work done on modeling the pebble beds in the FEM framework can be found in literature. [13, 14, 16, 21, 23–25]

Large-scale FEM models provide the only ability to move forward with system-integrated thermomechanical analysis of solid breeder volumes as they will interact with entire breeding modules. For example, many Parties participating with TBM designs in ITER have analyzed their units with FEM simulations. These major efforts will be discussed in another lecture by Dr. Alice Ying and so I won't include any examples here.

2.5 Discrete Modeling of Packed Beds

Aided by the acceleration and availability of computational power, many researchers of granular heat transfer have shifted their attention to studies of the interacting physics on pebble-scales with the discrete element method (DEM). In this approach, we interrogate heat transfer on the scale of contact conductance between interacting particles and directly model transient behaviors of packed beds. This approach has the advantage providing the capability to monitor transient changes to metastable packing structures of pebble beds; changes such as plastic rearrangement, inter-particle sintering/creep, fragmentation of pebbles, *etc.*.

DEM models have also been shown to efficiently couple to either volume-averaged fluid models or models of the entire tortuous fluid flow through the porous network of packed beds. Refs [5, 6, 20, 38, 59, 60] contain recent examples of application DEM models for solid breeder research.

2.5.1 Particle Dynamics

The grains in our system are allowed translational and rotational degrees of freedom. In a packed bed, we can restrict our attention to local forces between particles; neglecting, say, non-contact forces such as, van der Waals, electrostatic, or for the time being any fluid interaction forces. Assuming we know the contact forces acting upon particle i , Newton's equations of motion are sufficient to describe the particle

kinematics. For translation and rotational degrees of freedom, the equations are:,

$$m_i \frac{d^2 \vec{r}_i}{dt^2} = m_i \vec{g} + \vec{f}_i \quad (2.7a)$$

$$I_i \frac{d\vec{\omega}_i}{dt} = \vec{T}_i \quad (2.7b)$$

where m_i is the particle mass, \vec{r}_i its location in space, \vec{g} is gravity, I_i is the particle's moment of inertia, and $\vec{\omega}_i$ its angular velocity.

The net contact force, \vec{f}_i , represents the sum of the normal and tangential forces from the total number of contacts, Z , acting on this grain.

$$\vec{f}_i = \sum_{j=1}^Z \vec{f}_{n,ij} + \vec{f}_{t,ij} \quad (2.8)$$

and the net torque, \vec{T}_i , is similarly,

$$\vec{T}_i = -\frac{1}{2} \sum_{j=1}^Z \vec{r}_{ij} \times \vec{f}_{t,ij} \quad (2.9)$$

When Cundall & Strack first proposed the discrete element method, they used a linear spring-dashpot structure which saw normal and tangential forces written as,

$$\vec{f}_{n,ij} = k_{n,ij} \delta_{n,ij} \vec{n}_{ij} - \gamma_{n,ij} \vec{u}_{n,ij} \quad (2.10a)$$

$$\vec{f}_{t,ij} = k_{t,ij} \delta_{t,ij} \vec{t}_{ij} - \gamma_{t,ij} \vec{u}_{t,ij} \quad (2.10b)$$

where Cundall & Strack defined the stiffness coefficients k as constants and local damping coefficients γ were proportional to them, $\gamma \propto k$, to allow dissipation of energy and the system to reach an equilibrium.

Relative normal and tangential velocities, respectively, are decomposed from particle velocities,

$$\vec{u}_{n,ij} = (-(\vec{u}_i - \vec{u}_j) \cdot \vec{n}_{ij}) \vec{n}_{ij} \quad (2.11a)$$

$$\vec{u}_{t,ij} = (-(\vec{u}_i - \vec{u}_j) \cdot \vec{t}_{ij}) \vec{t}_{ij} \quad (2.11b)$$

with the unit vector \vec{n}_{ij} pointing from particle j to i

Surfaces of the two particles are allowed to virtually pass through each other (no deformation) resulting in normal and tangential overlaps of,

$$\delta_{n,ij} = (R_i + R_j) - (\vec{r}_i - \vec{r}_j) \cdot \vec{n}_{ij} \quad (2.12a)$$

$$\delta_{t,ij} = \int_{t_{c,0}}^t \vec{u}_{t,ij} d\tau \quad (2.12b)$$

where the fictive tangential overlap, $\delta_{t,ij}$, is truncated to so the tangential and normal forces obey Coulomb's Law, $\vec{f}_{t,ij} \leq \mu_i \vec{f}_{n,ij}$ with μ as the coefficient of friction of the particle.

Thus the approach of DEM is relatively simple: calculate interaction forces between particles with Equation (2.10) based on the kinematics of velocity and position of interacting particles from Equation (2.11) and Equation (2.12), respectively, then update the positions based on the forces. As DEM evolved and drew attention of more researchers, more complex formulas governing the spring-dashpot coefficients of Equation (2.10) emerged. But the core approach remained the same and the models all fall into the same family of so-called 'soft particle' models of DEM. A well-composed summary of the different DEM force models is given by Zhu et al.. [66]

The method used in this work fits into the computational skeleton of Cundall and Strack's method but with non-linear spring-dashpot coefficients defined by simplified Hertz-Mindlin-Deresiewicz model. In this model, the normal-direction stiffness coefficient of Equation (2.10a) is based on the Hertzian contact law. The tangential-direction stiffness coefficient follows from Brilliantov [8,37,66]. Together, the spring coefficients are,

$$k_{n,ij} = \frac{4}{3} E_{ij}^* \sqrt{R_{ij}^* \delta_{n,ij}} \quad (2.13a)$$

$$k_{t,ij} = 8G_{ij}^* \sqrt{R_{ij}^* \delta_{t,ij}} \quad (2.13b)$$

where E_{ij}^* is the pair Young's modulus, G_{ij}^* is the pair bulk modulus, and R_{ij}^* is the relative radius. The terms are defined as,

$$\frac{1}{E^*} = \frac{1 - \nu_1^2}{E_1} + \frac{1 - \nu_2^2}{E_2} \quad (2.14a)$$

$$\frac{1}{R^*} = \frac{1}{R_1} + \frac{1}{R_2} \quad (2.14b)$$

$$\frac{1}{G_{ij}^*} = \frac{2(2 + \nu_i)}{E_i} + \frac{2(2 + \nu_j)}{E_j} \quad (2.14c)$$

Similar to Cundall & Strack's formulation, damping coefficients, γ , are included to account for energy dissipated from the collision of two particles [17,53,54]. Whether the damping coefficient is local or global and the exact form of the coefficient is more important for loosely confined granular systems and dictates the way the system approaches an equilibrium state [40]. For the case of our tightly packed pebble

beds, it suffices to use the efficient form of Refs. [8, 40, 50, 65, 66],

$$\gamma_n = \sqrt{5} \beta_{\text{diss}} \sqrt{m^* k_{n,ij}} \quad (2.15a)$$

$$\gamma_t = \sqrt{\frac{10}{3}} \beta_{\text{damp}} \sqrt{k_{t,ij} m^*} \quad (2.15b)$$

with β_{damp} as the damping ratio, and the pair mass, $\frac{1}{m^*} = \frac{1}{m_i} + \frac{1}{m_j}$. For a stable system with $\beta_{\text{damp}} < 1$, the damping ratio is related to the coefficient of restitution, e , as

$$\beta_{\text{diss}} = -\frac{\ln e}{\sqrt{\ln^2 e + \pi^2}} \quad (2.16)$$

Systems to be solved by DEM models are therefore well-defined after specifying the few material properties of E , ν , ρ , and R_p and the interaction properties of μ and e .

Having expressed the contact mechanics of the discrete element method, we now must integrate the kinematic equations of the particles to resolve their evolutions. The most common means of marching in time with DEM is the velocity-Verlet algorithm [36]. In this algorithm, Equation (2.7) are integrated with half-steps in velocity, full steps in position, and then finally the full step in velocity. In practice, the two half-steps in velocity are often compressed into a single, full step.

2.5.2 Granular Heat Transfer in DEM

In a way analogous to handling particle momentums with Newton's laws of motion, Lagrangian tracking of particle energy is obtained *via* the first law of thermodynamics. Each particle is treated as a single distinct object and thus internal temperature gradients are assumed negligible. The temperature of particle i is governed by

$$m_i C_i \frac{dT_i}{dt} = Q_{s,i} + Q_i \quad (2.17)$$

where m and C are the mass and the specific heat of the solid, respectively. Heat generation inside the particle is input with Q_s and the total heat transferred to/from particle i *via* conduction to all, Z , neighboring particles, is

$$Q_i = \sum_{j=1}^Z Q_{ij} \quad (2.18)$$

Assuming the particles are spherical, smooth, elastic, in vacuum, and we neglect radiation transfer between them, for two particles at temperatures T_i and T_j , we

quantify the amount of energy transferred between them with a contact conductance, H_c :

$$Q_{ij} = H_c(T_i - T_j) \quad (2.19)$$

where H_c is a contact conductance term defining the squeezing of heat transfer through contact areas, [7,10]

$$H_c = 4k^*a = 4k^*\left(\frac{3}{4}\frac{R^*}{E^*}\right)^{1/3} F_n^{1/3} \quad (2.20)$$

where $\frac{1}{k^*} = \frac{1}{k_i} + \frac{1}{k_j}$ and $k_{i/j}$ are conductivities of contacting solids and a is the radius of contact. Because we have assumed smooth, elastic, spherical solids, with Hertz theory, contact radius can be found as a function of contact normal force, F_n ,

$$a = \left(\frac{3}{4}\frac{R^*}{E^*}\right)^{1/3} F_n^{1/3} \quad (2.21)$$

where, as before, $\frac{1}{E^*} = \frac{1-v_1^2}{E_1} + \frac{1-v_2^2}{E_2}$ and $\frac{1}{R^*} = \frac{1}{R_1} + \frac{1}{R_2}$.

The total heat transferred out of a single particle with Z contacts, due to contact conductance, is then simply the summed contribution of individual contacts,

$$Q_i = \sum_j^Z Q_{ij} \quad (2.22)$$

2.5.3 DEM Example Analysis

This section will use a recently published (in print) study we performed using DEM simulation coupled to a volume-averaged CFD code to highlight the information provided by DEM simulations. In the study, we considered the changes to heat transfer as packing structures evolve due to fragmentation of individual pebbles. Pebble fragmentation was considered by replacing individual pebbles with pebbles of smaller sizes. These smaller ‘fragments’ were free to move through interstitial gaps. We ran through a parametric space of initial packing fraction, fragment radius, and breeder volume orientation. For orientation, we considered pebble beds that were ‘standing up’ with vertical walls of heat transfer, and beds that were ‘lying down’ with heat transfer walls that were horizontal.

Using DEM, we tracked the displacement of fragments as they resettled in the beds. Figure 2.12 depict fragments after being placed into the system (Figure 2.12a) and after coming to rest (Figure 2.12b). Quantitatively, a histogram of normalized pebble travel is given in Figure 2.13. We found that long-distance travel of pebble

fragments yielded unintuitive consequences on heat transfer in packed beds (see the paper for more details).

Temperature distributions in pebble beds at cut-plane in the center of the bed are shown in Figure 2.14. The information from DEM was used to identify certain zones in pebble beds which showed different behavior during fragment resettling depending on the orientation of the pebble bed with respect to gravity. In Figures 2.15 and 2.16, the changes in packing fraction are shown (as averaged through this cross-sectional plane) for horizontal beds with different size fragments. These figures show the redistribution of mass (and therefore volumetric heating) as a function of amount of crushed pebbles.

This short review is meant to provide just a small glimpse of the power of DEM simulations (with some colorful pictures) and the wealth of information they provide for inter-particle interactions. The results presented here and the conclusions we were able to draw from them would not have been possible without the simulation scale of discrete element method models. For this reason, this approach remains as a main effort of many solid breeder research institutes around the world.

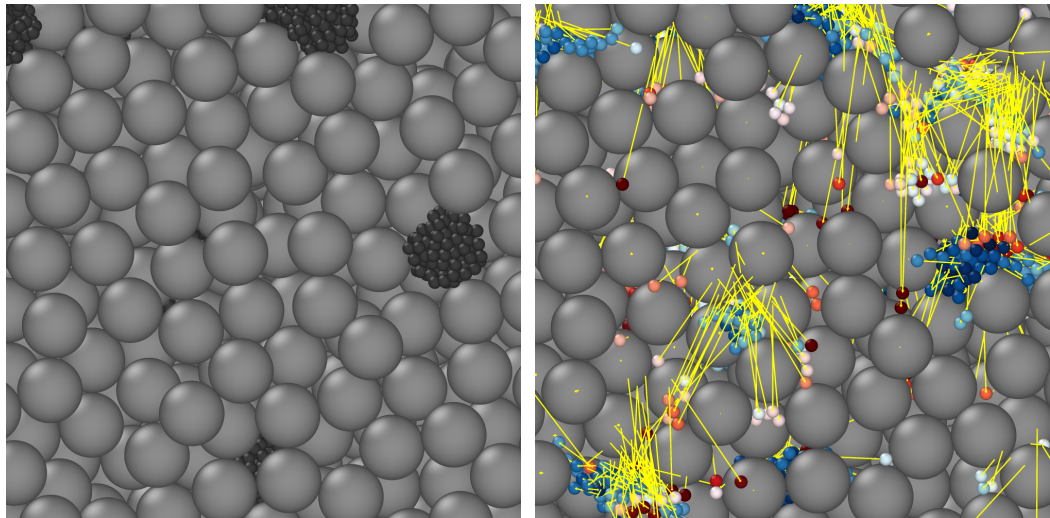


Figure 2.12: Vector displacements of fragments after resettling.

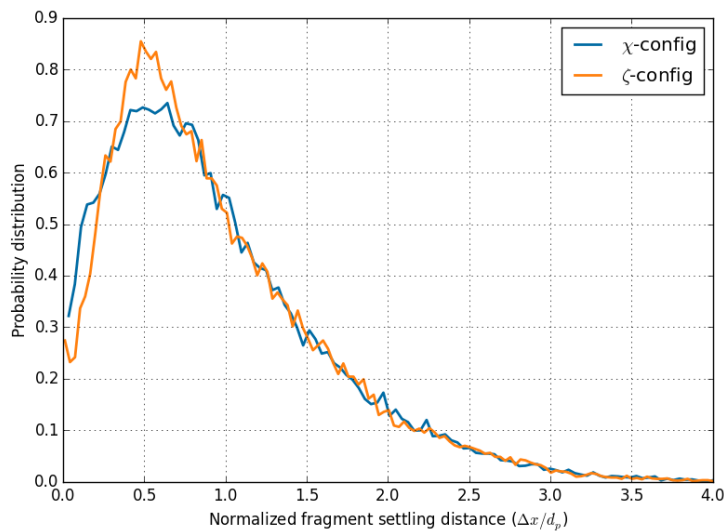


Figure 2.13: Normalized displacement histograms. χ -config: 59.7% of fragments travel up to 1 mm and 8.2% travel more than 2 mm; ζ -config: 60.7% of fragments travel up to 1 mm, 7.9% travel more than 2 mm.

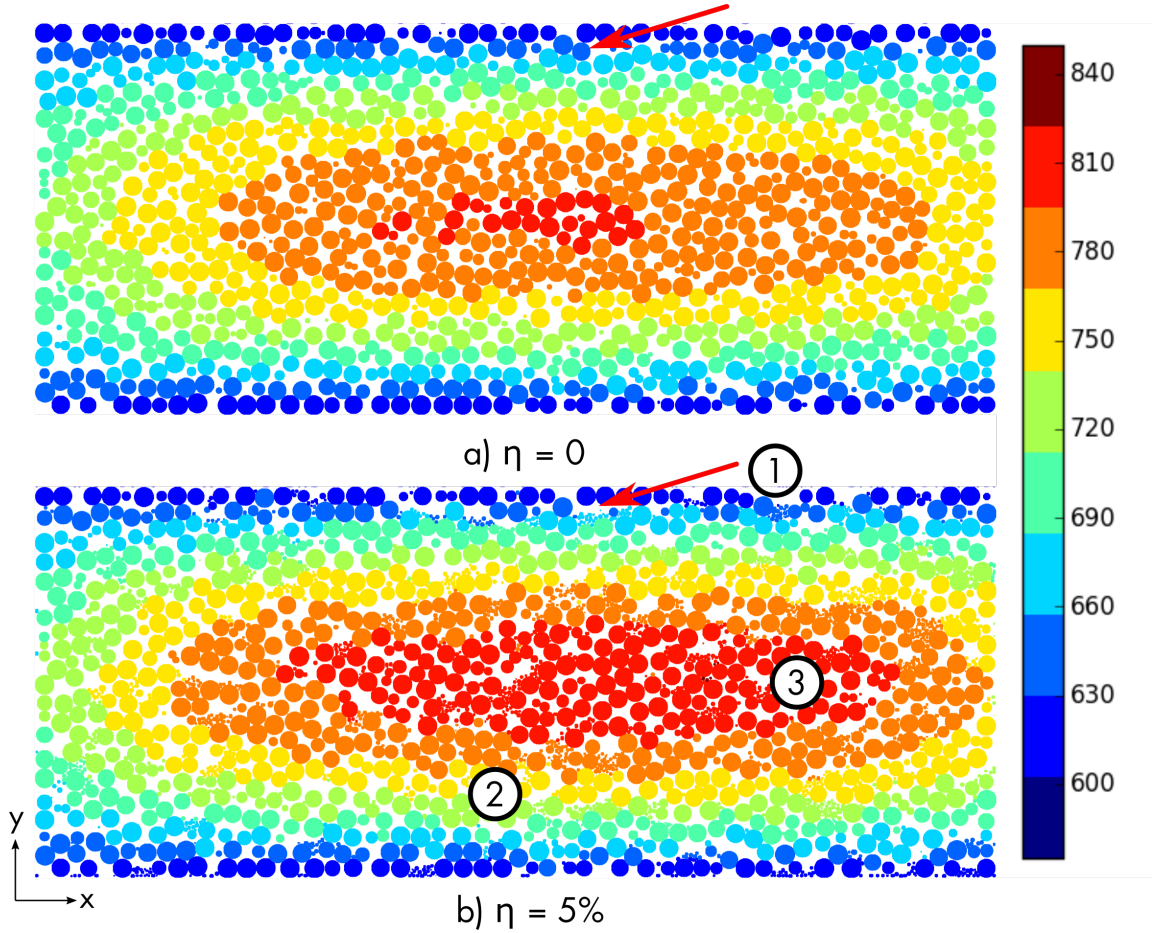


Figure 2.14: Cuts at the mid-plane of z for ζ -config beds. (a) bed initially packed to ϕ_2 , and (b) bed with crushing of η_5 pebbles with particle size r_2^* . Three important zones have been identified

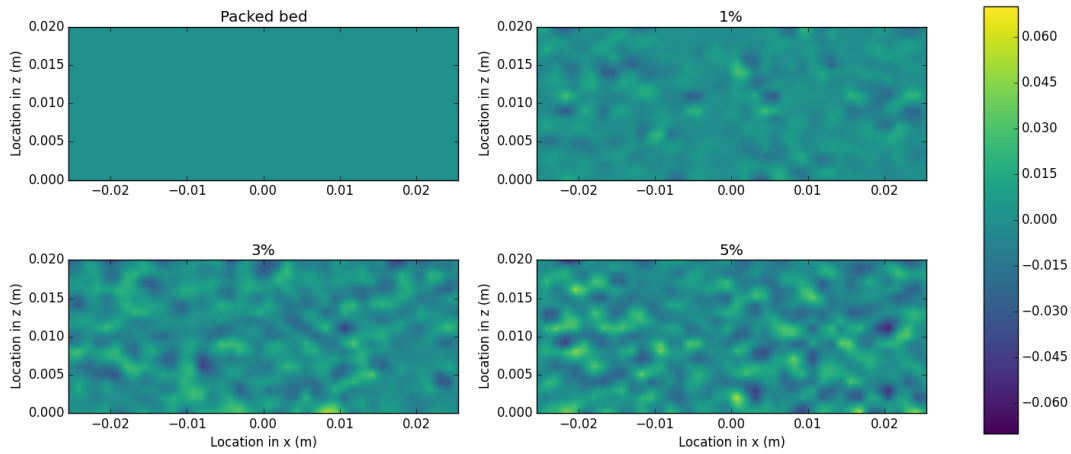


Figure 2.15: Distribution of local changes in packing fraction ($\phi_\eta - \phi_i$) for ζ -config, $\phi = 0.64$, $r^* = 0.32$

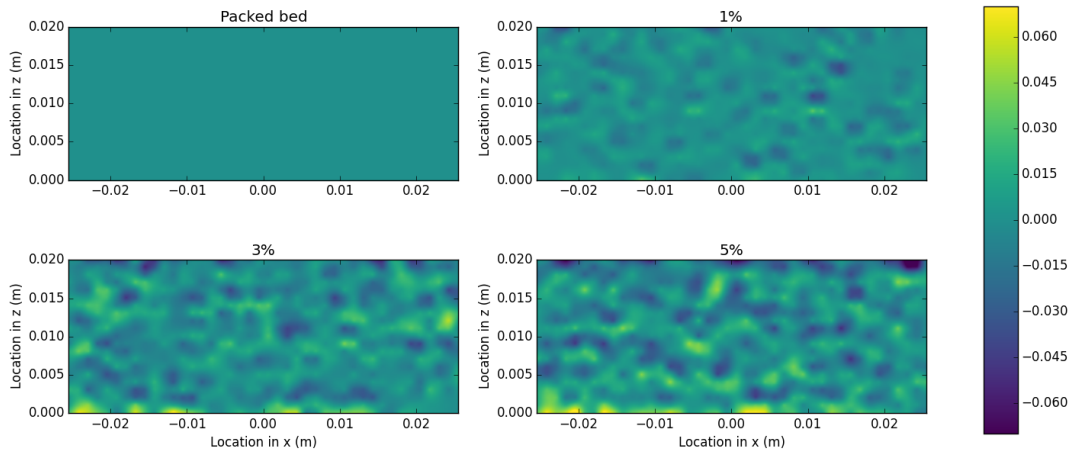


Figure 2.16: Distribution of local changes in packing fraction ($\phi_\eta - \phi_i$) for ζ -config, $\phi = 0.64$, $r^* = 0.2$

2.6 Closing Remarks

Pebble bed heat transfer appears deceptively simple. After all, the pebbles are meant to be stationary inside a fixed volume container. Yet the unique conditions of solid breeders operating in a fusion environment result in complicated heat transfer mechanisms that are still not fully understood or characterized. In this chapter, we introduced historical, phenomenological models of effective conductivity in packed beds as well as two methods of modeling packed beds specifically for solid breeders: (i) the continuum approach for large-scale FEM models and (ii) microscopic/discrete approach where we track individual pebbles in the ensemble. A full model of heat transfer of a solid breeder unit will, most likely, be a merger between these two approaches. Predictive capabilities for solid breeder pebble beds remains very much an open research topic.

Bibliography

- [1] Mohamed Abdou, Neil B. Morley, Sergey Smolentsev, Alice Ying, Siegfried Malang, Arthur Rowcliffe, and Mike Ulrickson. Blanket/first wall challenges and required R&D on the pathway to DEMO. *Fusion Engineering and Design*, 100:2–43, 2015.
- [2] Mohamed A Abdou, SE Berk, Alice Y. Ying, Martin YK Peng, S. Sharafat, JD Galambos, GW Hollenberg, Siegfried Malang, E Proust, Steven J Booth, L.M. Giancarli, P Lorenzetto, Yasushi Seki, V V Filatov, GE Shatalov, and A Sidorenkov. Results of an International Study on a High-Volume Plasma-Based Neutron Source for Fusion Blanket Development. *Fusion Technology*, 29:1–57, 1996.
- [3] Mohamed A Abdou, Layton J Wittenberg, and Charles W Maynard. A Fusion Design Study of Nonmobile Blankets with Low Lithium and Tritium Inventories. *Nuclear Technology*, 1975.
- [4] Ali Abou-Sena, Alice Y. Ying, and Mohamed A Abdou. Effective Thermal Conductivity of Lithium Ceramic Pebble Beds for Fusion Blankets: A Review. *Fusion Science and Technology*, 47(4):1094–1100, 2005.
- [5] Zhiyong An, Alice Y. Ying, and Mohamed A Abdou. Application of discrete element method to study mechanical behaviors of ceramic breeder pebble beds. *Fusion Engineering and Design*, 82(15-24):2233–2238, oct 2007.
- [6] Ratna Kumar Annabattula, Yixiang Gan, and Marc Kamlah. Mechanics of binary and polydisperse spherical pebble assembly. *Fusion Engineering and Design*, pages 2–7, mar 2012.
- [7] G.K. Batchelor and R.W. O'Brien. Thermal or Electrical Conduction Through a Granular Material. *Proceedings of the Royal Society of London. Series A, Mathematical and Physical Sciences*, 355(1682):313–333, 1977.

- [8] Nv Brilliantov, F Spahn, Jm Hertzsch, and T Pöschel. Model for collisions in granular gases. *Physical review. E, Statistical physics, plasmas, fluids, and related interdisciplinary topics*, 53(5):5382–5392, may 1996.
- [9] L. Bühler and Jörg Reimann. Thermal creep of granular breeder materials in fusion blankets. *Journal of Nuclear Materials*, 307-311:807–810, dec 2002.
- [10] G.J. Cheng, A.B. Yu, and P. Zulli. Evaluation of effective thermal conductivity from the structure of a packed bed. *Chemical Engineering Science*, 54(4199):4209, 1999.
- [11] RG Clemmer. The Development of Tritium Breeding Blankets for DT-Burning Fusion Reactors. In *Fourth ANS Topical Meeting on the Technology of Controlled Nuclear Fusion*, 1980.
- [12] R. G. Deissler and J. S. Boegli. An investigation of effective thermal conductivities of powders in various gases. *ASME Transactions*, 80(7):1417–1425, 1958.
- [13] G. Dell'Orco, Francesco Paolo Di Maio, R. Giannusso, A. Tincani, and G. Vella. On the theoretical-numerical study of the HEXCALIBER mock-up thermo-mechanical behaviour. *Fusion Engineering and Design*, 85(5):694–706, aug 2010.
- [14] G. Dell'Orco, P Dimaio, R. Giannusso, A. Tincani, G. Vella, and Francesco Paolo Di Maio. A constitutive model for the thermo-mechanical behaviour of fusion-relevant pebble beds and its application to the simulation of HELICA mock-up experimental results. *Fusion Engineering and Design*, 82(15-24):2366–2374, oct 2007.
- [15] Francesco Paolo Di Maio, G. Dell'Orco, R. Giannusso, A Malavasi, I. Ricapito, A. Tincani, and G. Vella. Experimental tests and thermo-mechanical analyses on the HEXCALIBER mock-up. *Fusion Engineering and Design*, 83(7-9):1287–1293, dec 2008.
- [16] Francesco Paolo Di Maio, R. Giannusso, and G. Vella. On the hyperporous non-linear elasticity model for fusion-relevant pebble beds. *Fusion Engineering and Design*, 85(7-9):1234–1244, 2010.
- [17] Alberto Di Renzo and Francesco Paolo Di Maio. Comparison of contact-force models for the simulation of collisions in DEM-based granular flow codes. *Chemical Engineering Science*, 59(3):525–541, feb 2004.
- [18] W. Dienst and H. Zimmermann. Investigation of the mechanical properties of ceramic breeder materials. *Journal of Nuclear Materials*, 155-157(PART 1):476–479, jul 1988.

- [19] J H Fokkens. Thermo-mechanical Finite Element Analyses for the HCPB In-pile Test Element, 2003.
- [20] Yixiang Gan, Francisco Hernandez, Dorian Hanaor, Ratna Kumar Annabattula, Marc Kamlah, and P. Pereslavtsev. Thermal Discrete Element Analysis of EU Solid Breeder Blanket Subjected to Neutron Irradiation. *Fusion Science & Technology*, 66(1), aug 2014.
- [21] Yixiang Gan and Marc Kamlah. Identification of material parameters of a thermo-mechanical model for pebble beds in fusion blankets. *Fusion Engineering and Design*, 82(2):189–206, feb 2007.
- [22] Yixiang Gan and Marc Kamlah. Thermo-mechanical analysis of pebble beds in HELICA mock-up experiments. *Fusion Engineering and Design*, 83(7-9):1313–1316, dec 2008.
- [23] Yixiang Gan and Marc Kamlah. Thermo-mechanical analyses of HELICA and HEXCALIBER mock-ups. *Journal of Nuclear Materials*, 386-388:1060–1064, apr 2009.
- [24] Yixiang Gan and Marc Kamlah. Thermo-mechanical modelling of pebble bed-wall interfaces. *Fusion Engineering and Design*, 85(1):24–32, jan 2010.
- [25] Yixiang Gan, Marc Kamlah, Heinz Riesch-Oppermann, Rolf Rolli, and Ping Liu. Crush probability analysis of ceramic breeder pebble beds under mechanical stresses. *Journal of Nuclear Materials*, pages 10–13, dec 2010.
- [26] L. Giancarli, V. Chuyanov, M. Abdou, M. Akiba, B.G. Hong, R. Lässer, C. Pan, and Y. Strebkov. Breeding Blanket Modules testing in ITER: An international program on the way to DEMO. *Fusion Engineering and Design*, 81(1-7):393–405, 2006.
- [27] Paul J Gierszewski. Review of properties of lithium metatitanate. *Fusion Engineering and Design*, 39-40:739–743, sep 1998.
- [28] J.B.J. Hegeman, E.D.L. van Essen, M. Jong, Jaap G van der Laan, and J. Reimann. Thermomechanical behaviour of ceramic breeder pebble stacks for HICU. *Fusion Engineering and Design*, 69(1-4):425–429, sep 2003.
- [29] G R Hopkins and R J Price. Fusion reactor design with ceramics. *Nuclear Engineering and Design*, 2:111–143, 1985.
- [30] Heinrich M. Jaeger, Sidney R. Nagel, and Robert P. Behringer. The Physics of Granular Materials. *Physics Today*, 49(4), 1996.

- [31] C.E. Johnson and RG Clemmer. Solid Breeder Materials. *Journal of Nuclear Materials*, 103 & 104:547–553, 1981.
- [32] C.E. Johnson, T. Kondo, N. Roux, Satoru Tanaka, and D. Vollath. Fabrication, properties, and tritium recovery from solid breeder materials. *Fusion Engineering and Design*, 16:127–139, dec 1991.
- [33] C.E. Johnson, K.R. Kummerer, and E. Roth. Ceramic breeder materials. *Journal of Nuclear Materials*, 155-157:188–201, jul 1988.
- [34] H Kawamura, E Ishitsuka, K Tsuchiya, M Nakamichi, M Uchida, H Yamada, K Nakamura, H Ito, T Nakazawa, H Takahashi, S Tanaka, N Yoshida, S Kato, and Y Ito. Development of advanced blanket materials for a solid breeder blanket of a fusion reactor. *Nuclear Fusion*, 43(8):675–680, aug 2003.
- [35] J.P. Kopasz, C.E. Johnson, and D.L. Baldwin. Performance of ceramic breeder materials in the SIBELIUS experiment. *Journal of Nuclear Materials*, 219:259–264, 1995.
- [36] H. Kruggel-Emden, M. Sturm, S. Wirtz, and V. Scherer. Selection of an appropriate time integration scheme for the discrete element method (DEM). *Computers & Chemical Engineering*, 32(10):2263–2279, oct 2008.
- [37] P A Langston, U Tlrzon, and D M Heyes. Discrete element simulation of granular flow in 2D and 3D hoppers: dependence of discharge rate and wall stress on particle interactions. *Chemical Engineering Science*, 50(6):967–987, 1995.
- [38] Zi Lu, Alice Y Ying, and Mohamed A Abdou. Numerical and experimental prediction of the thermomechanical performance of pebble beds for solid breeder blanket. *Fusion Engineering and Design*, 49-50:605–611, 2000.
- [39] A.J. Magielsen, M M W Peeters, J.B.J. Hegeman, M.P. Stijkel, and Jaap G van der Laan. Analysis of the in-pile operation and preliminary results of the post-irradiation dismantling of the pebble bed assemblies, presented at the 8th ISFNT, 2007.
- [40] Hernán Makse, Nicolas Gland, David Johnson, and Lawrence Schwartz. Granular packings: Nonlinear elasticity, sound propagation, and collective relaxation dynamics. *Physical Review E*, 70(6):061302, dec 2004.
- [41] G Piazza, Jörg Reimann, E Günther, Regina Knitter, N. Roux, and J D Lulewicz. Characterisation of ceramic breeder materials for the helium cooled pebble bed blanket. *Journal of Nuclear Materials*, 307-311(0):811–816, dec 2002.

- [42] Jörg Reimann, E. Arbogast, M. Behnke, S. Müller, and K. Thomauske. Thermo-mechanical behaviour of ceramic breeder and beryllium pebble beds. *Fusion Engineering and Design*, 49-50:643–649, 2000.
- [43] Jörg Reimann, Lorenzo Boccaccini, Mikio Enoeda, and Alice Ying. Thermomechanics of solid breeder and Be pebble bed materials. *Fusion Engineering and Design*, 61-62:319–331, nov 2002.
- [44] Jörg Reimann, D. Ericher, and G. Wörner. Influence of pebble bed dimensions and filling factor on mechanical pebble bed properties. *Fusion Engineering and Design*, 69(1-4):241–244, 2003.
- [45] Jörg Reimann and H. Harsch. Thermal creep of beryllium pebble beds. *Fusion Engineering and Design*, 75-79:1043–1047, nov 2005.
- [46] Jörg Reimann and S Hermsmeyer. Thermal conductivity of compressed ceramic breeder pebble beds. *Fusion Engineering and Design*, 61-62:345–351, nov 2002.
- [47] Jörg Reimann and G. Wörner. Thermal creep of Li₄SiO₄ pebble beds. *Fusion Engineering and Design*, 58-59:647–651, nov 2001.
- [48] N. Roux, J.J. Abassin, M. Briec, D. Cruz, T. Flament, and I. Schuster. Compatibility behavior of beryllium with LiAlO₂ and Li₂ZrO₃ ceramics, with 316 L and 1.4914 steels in SIBELIUS. *Journal of Nuclear Materials*, 191-194:168–172, 1992.
- [49] N. Roux, Satoru Tanaka, C.E. Johnson, and R Verrall. Ceramic breeder material development. *Fusion Engineering and Design*, 41(1-4):31–38, 1998.
- [50] J. Shafer, S Dippel, and D. E. Wolf. Force Schemes in Simulations of Granular Materials. *Journal de Physique I*, 6(1):5–20, jan 1996.
- [51] L. L. Snead, S. J. Zinkle, and D. P. White. Thermal conductivity degradation of ceramic materials due to low temperature, low dose neutron irradiation. *Journal of Nuclear Materials*, 340(2-3):187–202, 2005.
- [52] Hisashi Tanigawa, Mikio Enoeda, and Masato Akiba. Measurement of thermal expansion of Li₂TiO₃ pebble beds. *Fusion Engineering and Design*, 82(15-24):2259–2263, oct 2007.
- [53] Y. Tsuji, T. Kawaguchi, and T. Tanaka. Discrete particle simulation of two-dimensional fluidized bed. *Powder Technology*, 77(1):79–87, oct 1993.
- [54] Y. Tsuji, T. Tanaka, and T Ishida. Lagrangian numerical simulation of plug flow of cohesionless particles in a horizontal pipe. *Powder Technology*, 71(3):239–250, sep 1992.

- [55] W. van Antwerpen, C.G. du Toit, and P.G. Rousseau. A review of correlations to model the packing structure and effective thermal conductivity in packed beds of mono-sized spherical particles. *Nuclear Engineering and Design*, 240(7):1803–1818, jul 2010.
- [56] Jaap G van der Laan, Alexander Fedorov, Sander van Til, and Jörg Reimann. Ceramic Breeder Materials. Technical report, 2011.
- [57] Jaap G van der Laan, Hiroshi Kawamura, N. Roux, and D Yamaki. Ceramic breeder research and development: progress and focus. *Journal of Nuclear Materials*, 283-287(0):99–109, dec 2000.
- [58] D van Houtte, K Okayama, and F Sagot. ITER operational availability and fluence objectives. *Fusion Engineering and Design*, 86(6-8):680–683, oct 2011.
- [59] Jon Thomas Van Lew, Alice Ying, and Mohamed Abdou. Coupling Discrete Element Models of Ceramic Breeder Pebble Beds to Thermofluid Models of Helium Purge Gas Using Volume-Averaged Navier-Stokes and the Lattice-Boltzmann Method. *Fusion Science and Technology*, 68(2):288–294, sep 2015.
- [60] Jon Thomas Van Lew, Alice Ying, and Mohamed A Abdou. A discrete element method study on the evolution of thermomechanics of a pebble bed experiencing pebble failure. *Fusion Engineering and Design*, 89(7-8):1151–1157, oct 2014.
- [61] S. van Til, A.V. Fedorov, and A.J. Magielsen. Study of ceramic pebble beds in Post Irradiation Examination of the Pebble Bed Assemblies irradiation experiment. *Fusion Engineering and Design*, 87(5-6):885–889, aug 2012.
- [62] P. Zehner and E. U. Schlünder. Wärmeleitfähigkeit von Schüttungen bei mäßigen Temperaturen. *Chemie Ingenieur Technik - CIT*, 42(14):933–941, jul 1970.
- [63] P. Zehner and E. U. Schlünder. Einfluß der Wärmestrahlung und des Druckes auf den Wärmetransport in nicht durchströmten Schüttungen. *Chemie Ingenieur Technik - CIT*, 44(23):1303–1308, 1972.
- [64] Chunbo Zhang, Alice Ying, and Mohamed Abdou. FEM Modeling of Pebble Bed/Structural Wall Separation. *Fusion Science and Technology*, 68(3):612–617, oct 2015.
- [65] H. Zhang and Hernán Makse. Jamming transition in emulsions and granular materials. *Physical Review E*, 72(1):011301, jul 2005.
- [66] H.P. Zhu, Z.Y. Zhou, R.Y. Yang, and A.B. Yu. Discrete particle simulation of particulate systems: Theoretical developments. *Chemical Engineering Science*, 62(13):3378–3396, jul 2007.